J. Fluid Mech. (1995), *vol.* 289, *pp.* 315–349

Effects of soluble and insoluble surfactant on laminar interactions of vortical flows with a free surface

By WU-TING TSAI † AND DICK K. P. YUE

Department of Ocean Engineering, Massachusetts Institute of Technology, Cambridge, MA 02139, USA

(Received 16 May 1994 and in revised form 23 November 1994)

We study the two-dimensional, laminar interactions between a contaminated free surface and a vortical flow below. Two canonical vortical flows are considered: a pair of vortex tubes impinging onto the free surface; and an unstable shear wake behind a body operating on the surface. A quantitative model for free-surface viscous flows in the presence of soluble or insoluble surfactants is developed. For the low to moderate Froude numbers considered here, for which weakly nonlinear free-surface boundary conditions are valid, the surface boundary layer and vorticity production are weak for *clean* water and the vortical flow evolution does not differ qualitatively from that under a free-slip boundary. When even a small amount of contamination is present, the flow can be dramatically affected. The vortical flow creates gradients in the surfactant surface concentration which leads to Marangoni stresses, strong surface vorticity generation, boundary layers, and even separation. These significantly influence the underlying flow which itself affects surfactant transport in a closed-loop interaction. The resulting flow features are intermediate between but qualitatively distinct from those under either a free- or no-slip boundary. Surfactant effects are most prominent for insoluble surface contamination with likely development of surfactant shocks and associated surface features such as Reynolds ridges. For soluble surfactant with initially uniform bulk concentration, surface concentration variations are moderated by sorption kinetics between the surface and bulk phases, and the overall effects are generally diminished. For initially stratified bulk concentrations, however, the evolution dynamics becomes more varied and surfactant effects may be amplified relative to the insoluble case. The dependence of these results on the properties of the contamination is studied.

1. Introduction

The behaviour of vortical flows near a free surface is complex due to the dynamic couplings among the effects associated with the deformable boundary, viscosity and surface stresses. In the real ocean or laboratory settings, the situation is further complicated by contamination of surface-active material (surfactant) on the free surface which may significantly affect the underlying flow.

Without considering possible surfactant effects, Barker & Crow (1977) used a free surface to model a stress-free boundary in their experiment on ground effects on

† Present address: Department of Oceanography, Ocean University, Keelung, Taiwan, ROC.

the motion of a vortex pair. Apparently due to the presence of contamination, they observed 'rebounding' of the impinging vortex pair for both a free surface and a solid boundary, and concluded that both boundaries have similar effects on the motions. More recent experiments by Bernal *et al.* (1989) showed that the rebounding effect of a vortex ring or pair impinging a free surface was much reduced when the free surface was cleaned by draining. Further experiments and computations by Hirsa *et al.* (1990) for a vortex pair confirm that contamination is the cause of dramatic changes in the resulting vortical motions. Numerical studies incorporating the effect of *insoluble* surfactant contamination on the surface/vortex pair interaction were conducted by Wang & Leighton (1990) and Tryggvason *et al.* (1992) in which the free surface was assumed to be flat, and by Yeung & Ananthakrishnan (1992) who considered nonlinear effects. These numerical studies largely confirm the experimental observations of Bernal *et al.* (1989) and Hirsa *et al.* (1990).

The differences in the effects of clean and contaminated surfaces on the underlying vortical flows are due to the well-known Marangoni effect which is a closed-loop interaction among the hydrodynamic motion, surfactant concentration transport and surface tension. The presence of surface agents generally lowers the local interfacial tension. Hydrodynamic disturbances result in a non-uniform distribution of surfactant concentration on the free surface, and consequently local interfacial tension gradients are created. The resulting shear stresses on the free surface lead to strong surface vorticity generation which interacts with and changes the structure of the bulk flow.

To understand and quantify these effects and the dependence on the surfactant properties, we develop a quantitative description and model for free-surface viscous flows in the presence of soluble or insoluble surfactant. The degree of surface activity of contamination depends on the surface sorption and mixing in the aqueous phase. In general, inorganic ions in water are attracted into the aqueous phase and are thus soluble. (If an ionic solution is very dilute, the Gouy–Chapman double layer can be quite thick and then ions behave as if very surface-active (Harper 1974).) On the other hand, typical organic compounds with a long-chain hydrocarbon tail and a polar head are relatively insoluble. The present model includes convection-diffusion-sorption processes governing the evolutions of bulk and interfacial surfactant compositions and their coupling to the vortical flow dynamics through the stress boundary conditions. The coupling mechanism between the surfactant transport and the free-surface flow is given via the equation of state which relates the surfactant concentration to the surface tension. The boundary-value problem governing the viscous free-surface flow, the transport of soluble and insoluble surfactants, and the coupling equation of state are given in §§2 – 4.

In numerical simulation, it is often necessary and desirable to make simplifying linearizations of the free-surface boundary conditions based on presumed scales for the associated lengths and velocities. In §5, a set of weakly nonlinear free-surface conditions and surfactant transport equations are derived based on two vertical length scales corresponding to the thickness of the free-surface boundary layer and the amplitude of the free-surface motion respectively. The weakly nonlinear free-surface boundary conditions include the production of free-surface vorticity associated with diffusion, unsteadiness, convection, Marangoni effect, and surfactant viscosity, in addition to the classic 'curvature effect' term of Batchelor (1967) and Lugt (1987). The numerical method and implementation for solving the coupled viscous free-surface flow and surfactant transport equations are then described in §6.

Guided in part by existing experimental investigations, we first study, as a canonical problem, a pair of vortex tubes parallel to the free surface and impinging on it. For

comparison, the clean surface case is first considered in §7.1. We then focus our attention on the effects of soluble and insoluble surfactants in §7.2. Of special note is the effect of solubility which has not been addressed in previous simulations. In §7.3 we examine in some detail the effects of the various properties affecting surfactant transport and in particular the adsorption/desorption kinetics of the soluble surfactant.

In the real ocean (or some laboratory) environment, the effect of surfactant solubility is further complicated by the (initial) variations of the bulk concentration caused either by bulk-phase temperature and density stratifications, or the nature and location of the contamination source. In §7.4 we consider initial bulk concentrations that are vertically stratified. The evolution dynamics become more varied and overall surfactant effects may be either amplified or diminished depending on the initial bulk distribution.

Finally, in §8, we consider the effects of surfactant on the development of an unstable free-surface shear wake. This problem was studied by Triantafyllou & Dimas (1989) and Dimas & Triantafyllou (1994) (see also Dimas 1991) who considered the inviscid case. At low Froude numbers, they identified two distinct regimes of linear instability corresponding respectively to low (mode I) and high (mode II) wavenumber disturbances. In the present study, we simulate the cases in Dimas & Triantafyllou (1994) but include the effects of viscosity and surfactants. As expected, the effect of viscosity is small for moderate Reynolds numbers, but the effect of even a small amount of surface contamination is dramatic especially for mode I interactions.

We should point out that the Marangoni effect is a well-known mechanism in the classical context of damping of surface waves by spreading films (see, for example, van den Tempel 1965, and more recently, Alpers & Hühnerfuss 1989; Lucassen 1982). These studies emphasize primarily interactions between the surface motions and surfactant transport, and their consequence in terms of attenuation of surface waves. In the present work, the focus is on *local* surface features and the accompanying evolution of underlying vortical structures. Such Marangoni effect mechanisms of free-surface interactions with primary vortical structures have only recently been of research interest, motivated by experimental observations such as Bernal *et al.* (1989).

In this study, we consider only two-dimensional interactions. The formulations and computational method developed can be extended to three-dimensional flows in a straightforward way. New physical mechanisms are introduced, however, associated with vortex stretching, turning and connection and, to a lesser degree, with three-dimensional surface deformations. The interaction features and modification of underlying vortical structures due to Marangoni effect will be more complex and drastic. These are subjects of current investigations.

2. Viscous free-surface flow

We consider the motions of a two-dimensional, viscous and incompressible bulk flow, and a free surface with or without surfactant contamination. In the following formulation, all variables are normalized by a characteristic length L, a velocity scale U, and the density of the bulk fluid ρ. The motions of the bulk flow are described by continuity and Navier–Stokes equations:

$$u_x + w_z = 0, \tag{2.1}$$

and

$$\frac{\partial u}{\partial t} + uu_x + wu_z + p_x - \frac{1}{\mathscr{R}_e}(u_{xx} + u_{zz}) = 0, \tag{2.2}$$

$$\frac{\partial w}{\partial t} + uw_x + ww_z + p_z - \frac{1}{\mathscr{R}_e}(w_{xx} + w_{zz}) = 0, \tag{2.3}$$

where u and w are horizontal and vertical velocities respectively, p the dynamic pressure, $\mathscr{R}_e = UL/\nu$ the Reynolds number, and ν the kinematic viscosity of the bulk fluid.

On the free surface ($z = \eta$), the boundary moves as a material surface which gives the kinematic boundary condition

$$\frac{\partial \eta}{\partial t} + u\eta_x - w = 0 \qquad \text{on} \quad z = \eta, \tag{2.4}$$

where η is the free-surface elevation. The conservation of linear momentum on the free surface gives rise to stress conditions imposed upon the contiguous bulk-flow stress fields. The complete derivation of the stress conditions for a Newtonian interface was given in Scriven (1960) and more recently in Edwards, Brenner & Wasan (1991). Resolving the stress condition into the tangential and normal components respectively yields the tangential and normal stress conditions:

$$\begin{aligned}
&\frac{1}{\mathscr{R}_e}\frac{1}{\mathscr{N}^2}\left[-2\eta_x(u_x - w_z) + (1-\eta_x^2)(u_z + w_x)\right] \\
&\quad = \frac{1}{\mathscr{W}_e}\frac{\sigma_x}{\mathscr{N}} + \frac{\mathscr{B}_o}{\mathscr{R}_e}\frac{1}{\mathscr{N}^3}\left[u_{xx} + \eta_x(2u_{xz} + w_{xx}) + \eta_x^2(u_{zz} + 2w_{xz}) + \eta_x^3 w_{zz}\right] \\
&\qquad - \frac{\mathscr{B}_o}{\mathscr{R}_e}\frac{\eta_{xx}}{\mathscr{N}^5}\left[2\eta_x(u_x - w_z) + (\eta_x^2 - 1)(u_z + w_x)\right],
\end{aligned} \tag{2.5}$$

and

$$\begin{aligned}
&-p + \frac{1}{\mathscr{F}_r^2}\eta + \frac{1}{\mathscr{R}_e}\frac{2}{\mathscr{N}^2}\left[\eta_x^2 u_x + w_z - \eta_x(u_z + w_x)\right] \\
&\qquad = \frac{\eta_{xx}}{\mathscr{N}^3}\left[\frac{\sigma}{\mathscr{W}_e} + \frac{\mathscr{B}_o}{\mathscr{R}_e}\frac{1}{\mathscr{N}^2}\left(u_x + \eta_x^2 w_z + \eta_x(u_z + w_x)\right)\right],
\end{aligned} \tag{2.6}$$

on $z = \eta$, with $\mathscr{N} = (1 + \eta_x^2)^{1/2}$, and σ the surface tension normalized by the equilibrium tension σ_0. The non-dimensional parameters in the equations are: Froude number $\mathscr{F}_r = U/(gL)^{1/2}$, Weber number $\mathscr{W}_e = \rho U^2 L/\sigma_0$ and Boussinesq number $\mathscr{B}_o = (\delta^s + \nu^s)/(\nu L)$, where δ^s and ν^s are respectively the surface dilational and shear kinematic viscosities of the surfactant. The free-surface boundary conditions (2.4)–(2.6) are nonlinear equations on $z = \eta$. Linearization of these conditions on $z = 0$ for the present numerical simulations will be discussed in §5.

3. Transport of soluble and insoluble surfactants

Conservation of surfactant molecules in a two-dimensional continuous medium gives the advection-diffusion equation for the bulk concentration $c(x, z, t)$:

$$\frac{\partial c}{\partial t} + uc_x + wc_z - \frac{1}{\mathscr{P}_e}(c_{xx} + c_{zz}) = 0, \tag{3.1}$$

where c is non-dimensionalized by the equilibrium uniform concentration c_0. The bulk-phase Péclet number $\mathscr{P}_e$ is defined as $\mathscr{P}_e = UL/D$, where D is the molecular

diffusivity of the surfactant. For the surface surfactant concentration $\gamma(x,t)$, the transport equation is (see for example Edwards *et al.* 1991) :

$$\frac{\partial \gamma}{\partial t} + \frac{1}{\mathscr{N}^2}\left[(u\gamma)_x + \eta_x(\gamma u_z + (w\gamma)_x) + \eta_x^2 \gamma w_z\right] - \frac{1}{\mathscr{P}_e^s}\left(\frac{\gamma_{xx}}{\mathscr{N}^2} - \frac{\eta_x \eta_{xx}}{\mathscr{N}^4}\gamma_x\right) = F, \tag{3.2}$$

where γ is normalized by the equilibrium uniform surface concentration γ_0, and $\mathscr{P}_e^s = UL/D^s$ is the surface Péclet number, and D^s the surface diffusivity of the surface-adsorbed surfactant. F is the normal diffusive flux of surfactant from the bulk phase, which according to Fick's law of diffusion, can be expressed as

$$F = -\frac{1}{\mathscr{P}_e}\frac{1}{\mathscr{K}}\left[-\frac{\eta_x}{\mathscr{N}}\frac{\partial c}{\partial x} + \frac{1}{\mathscr{N}}\frac{\partial c}{\partial z}\right]_{z=\eta}, \tag{3.3}$$

where $\mathscr{K} = \gamma_0/Lc_0$ is the non-dimensional equilibrium ratio between bulk and surface concentrations. For insoluble surfactant, there is no diffusive flux of surfactant from the bulk fluid, i.e. $F = 0$, and the surface-concentration equation (3.2) is solved independently of the bulk-concentration equation (3.1). Note that (3.2) and (3.3) are nonlinear equations applied on $z = \eta$. For the present simulations, a linearized form of these equations applied on $z = 0$ is employed (see §5).

Solution of the surface- and bulk-concentration transport equations (3.1) and (3.2) requires a constitutive equation for the interfacial flux transport F. This means that a kinetic-rate expression is required for F at the interface in terms of local surface and substrate bulk (bulk concentration at the free surface) concentrations. Such a constitutive expression in general depends on a large number of factors including the physico-chemical properties of the surfactant, equilibrium conditions, and thermodynamic ideality of the interface and bulk phase (see, for example, Borwanker & Wasan 1983, and the review by Lucassen-Reynders 1981). In the present study we adopt two classical adsorption isotherms which assume non-ionic surfactant, and thermodynamically ideal bulk fluid and equilibrium conditions.

The simplest kinetic expression is the linear rate equation:

$$F = \frac{1}{\mathscr{P}_e}\frac{1}{\mathscr{K}}\frac{1}{\mathscr{T}}(c - \gamma), \tag{3.4}$$

where the equilibrium ratio $\mathscr{K}$ is equal to the ratio of adsorption to desorption rates, $\mathscr{K} = \gamma_0/(Lc_0) = \kappa_a/(L\kappa_d)$. Here κ_a and κ_d are the rate constants for adsorption and desorption respectively. Note that $\mathscr{K}$ measures the degree of solubility: for decreasing $\mathscr{K}$, the surfactant become more soluble in the substrate; while for large $\mathscr{K}$, the surfactant adsorbs preferentially on the free surface. The equilibrium relation $\mathscr{K} = 1$ (i.e. $\kappa_a c_0 = \kappa_d \gamma_0$) can be assumed to obtain the instantaneous condition for c_0 and γ_0 which is the so-called Henry isotherm. In (3.4), $\mathscr{T} = D/(\kappa_a L)$ is the interfacial transport rate number. For small $\mathscr{T}$, the kinetics is the so-called diffusion-controlled adsorption. In this limit surfactant transport by diffusion is slow and adsorption can be considered to occur instantaneously relative to the diffusion process. In the limit of large $\mathscr{T}$, the surfactant is transported rapidly to the interface by diffusion and the kinetics is known as absorption-controlled transport.

For nonlinear adsorption kinetics, we focus on the expression which leads to the familiar Langmuir isotherm for equilibrium adsorption:

$$c_0 = \frac{\tilde{\kappa}_d}{\tilde{\kappa}_a}\frac{\gamma_0}{\gamma_\infty - \gamma_0} \equiv \frac{\tilde{\kappa}_d}{\tilde{\kappa}_a}\frac{1}{\beta}, \tag{3.5}$$

where γ_∞ is the saturation surface concentration. The kinetics expression for such a

nonlinear isotherm is

$$F = \frac{1}{\mathscr{P}_e}\frac{1}{\mathscr{K}}\frac{1}{\mathscr{T}}\left(\frac{\beta}{1+\beta}\right)\left[c\left(1+\frac{1-\gamma}{\beta}\right)-\gamma\right]. \tag{3.6}$$

Note that when $\beta \to \infty$ the nonlinear expression becomes the linear kinetics (3.4).

In summary, the transport of soluble surfactant is governed by $\mathscr{P}_e$, $\mathscr{P}_e^s$, $\mathscr{K}$ and $\mathscr{T}$ for linear adsorption kinetics, and an additional parameter β for nonlinear kinetics. The transport is in general further affected by motions of the bulk phase through advection and by free-surface deformations. To gain some quantitative understanding of the effects of the physical parameters, it is instructive to consider first the diffusion-sorption transport in the absence of hydrodynamic convection and surface deformations. Specifically, we study the one-dimensional initial-boundary-value problem in the vertical (z) direction of the transport equations (3.1) and (3.2) with $u, w, \eta \equiv 0$. (The numerical scheme for the diffusion-sorption transport problem is described in §6.) Initially, the bulk-surfactant concentration is assumed to be uniform ($c = 1$) in the entire depth and the surface concentration γ is set to zero. To quantify the rate of transport, an equilibrium time $t_e = t_e(\mathscr{P}_e, \mathscr{K}, \mathscr{T}, \beta)$ is defined to be that required for the surface concentration γ to reach 95% of the final equilibrium concentration ($\gamma = 1$). Following Pierson & Whitaker (1976), who studied the transport problem in a growing spherical drop, we present t_e as a function of the interfacial rate number $\mathscr{T}$ for varying $\mathscr{P}_e$, $\mathscr{K}$ and β in figure 1.

Figure 1(a) shows the dependence of t_e on $\mathscr{T}$ for varying degrees of nonlinearity β of the sorption kinetics. For $\mathscr{T}$ less than around 0.01, the transport kinetics are diffusion controlled, and the equilibrium time is independent of the adsorption kinetics. Increasing nonlinearity of the kinetic isotherm (decreasing β) reduces the equilibrium time. This is consistent with the calculations of Miller (1981) and differs from those of Pierson & Whitaker (1976) in which the equilibrium time is independent of nonlinearity. For large diffusion-adsorption rate $\mathscr{T}$, the transport is adsorption controlled. The existence of a kinetic resistance to the surfactant transport increases the time needed to reach an equilibrium state. The dependence of surfactant transport on the bulk Pélect number $\mathscr{P}_e$ is shown in figure 1(b). The equilibrium time decreases with increasing bulk-surfactant diffusivity D (decreasing Pélect number). For decreasing equilibrium surface bulk-concentration ratio $\mathscr{K}$, the equilibrium time also decreases as shown in figure 1(c). In this case, the small-$\mathscr{K}$ limit corresponds to high solubility and weak adsorption.

4. Equation of state

In the presence of surfactant contamination, the surface-tension variation is related to the surfactant surface concentration γ through a surface equation of state. For insoluble surfactants, quantitative experimental data are well documented (e.g. Gaines 1966). Here we assume a linear variation of the surface tension with the surfactant concentration around their equilibrium points, i.e.

$$\sigma - 1 = \frac{\gamma_0}{\sigma_0}\left(\frac{\mathrm{d}\sigma}{\mathrm{d}\gamma}\right)_{\gamma=1}(\gamma - 1) \equiv \mathscr{M}_a(1-\gamma), \tag{4.1}$$

where $\mathscr{M}_a \equiv (\gamma_0/\sigma_0)(\mathrm{d}\sigma/\mathrm{d}\gamma)_{\gamma=1}$ is the Marangoni number for the surfactant.

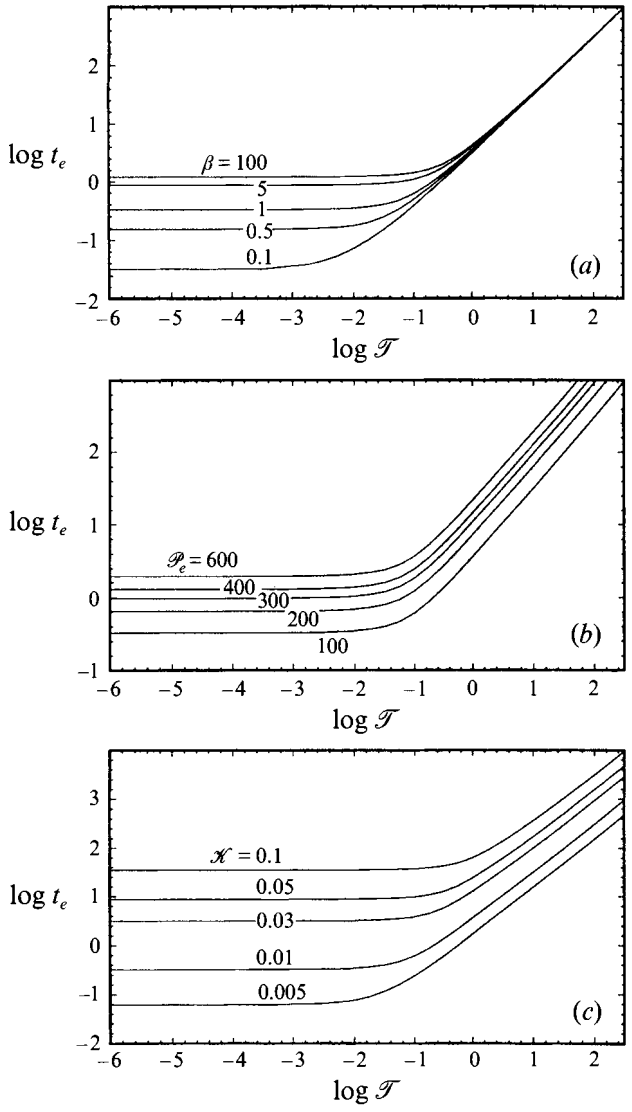

FIGURE 1. Equilibrium time t_e as a function of interfacial rate transport number $\mathscr{T}$ for varying: (*a*) kinetic nonlinearity β ($\mathscr{P}_e = 100$, $\mathscr{K} = 0.01$); (*b*) Pélect number $\mathscr{P}_e$ ($\beta = 1$, $\mathscr{K} = 0.01$); and (*c*) equilibrium coefficient $\mathscr{K}$ ($\beta = 1$, $\mathscr{P}_e = 100$).

For soluble surfactant, Gibbs' adsorption equation provides an equilibrium relationship between the surface tension and the surface concentration:

$$\sigma - 1 = RT\frac{\gamma_0}{\sigma_0}\int_1^{\gamma}\frac{\gamma}{c}\frac{\mathrm{d}c}{\mathrm{d}\gamma}\mathrm{d}\gamma, \tag{4.2}$$

where σ_0 is the equilibrium surface tension, R the gas constant, and T the absolute temperature. Such an equilibrium relationship is usually assumed to be applicable to non-equilibrium kinetics involving instantaneous surfactant adsorption. For a linear

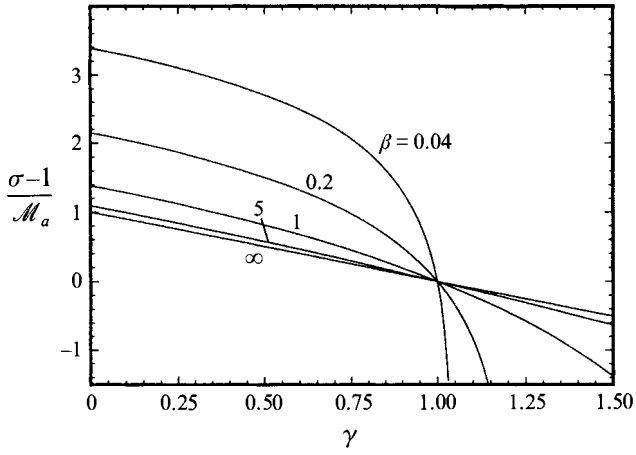

FIGURE 2. Surface tension $(\sigma - 1)/\mathcal{M}_a$ as a function of surface concentration γ for varying kinetic nonlinearity β.

(Henry) isotherm, (4.2) becomes

$$\sigma - 1 = RT\frac{\gamma_0}{\sigma_0}(1 - \gamma) \equiv \mathcal{M}_a(1 - \gamma). \tag{4.3}$$

For a nonlinear (Langmuir) isotherm, the equation of state becomes

$$\sigma - 1 = RT\frac{\gamma_0}{\sigma_0}(1 + \beta)\ln\left(\frac{1 + \beta - \gamma}{\beta}\right) \equiv \mathcal{M}_a(1 + \beta)\ln\left(\frac{1 + \beta - \gamma}{\beta}\right). \tag{4.4}$$

In figure 2 we show the surface-tension variation $(\sigma - 1)/\mathcal{M}_a$ versus surface concentration γ for different β. For nonlinear adsorption kinetics (small β), the surface tension decreases exponentially as surface concentration increases. As β increases, the curve converges to the linear equation of state (4.3).

The dependence of surface tension on the surfactant composition and the diffusion-sorption kinetics in the previous section are still among subjects of active research by surface physical chemists. A recent detailed review with updated references is given by Barger (1991). Here we have adopted the commonly used models to obtain a simple mathematical formulation for numerical simulation. The focus of the present study is on the coupling mechanisms between the hydrodynamics and the contamination transport but not specifically on the detailed interfacial processes themselves. Although more sophisticated and complicated expressions and experimental data may be used for the equation of state and the diffusion-sorption kinetics, the models we employ in the present study are adequate for the stated objective. In any event, a framework is provided in which more advanced models can be readily incorporated, evaluated and compared.

5. Perturbation approximation and surface vorticity production

To better understand the importance of the vortical flow and the surfactant in the free-surface interactions, we consider the role of the different hydrodynamic and surfactant effects on the production of free-surface vorticity. To facilitate the analysis, we assume that the free-surface boundary layer is of thickness $O(\delta)$, and the surface

deformations are of $O(\epsilon)$, with $\delta, \epsilon \ll 1$. Continuity within the boundary layer then requires $w/u \sim O(\delta)$ and momentum balance gives $\delta \sim O(\mathscr{R}_e^{-1/2})$.

For consistency, we assume $O(\delta) > O(\epsilon) > O(\delta^2)$ and carry out the perturbation and expansion about $z = 0$ systematically. The kinematic condition up to $O(\epsilon)$ is

$$\frac{\partial \eta}{\partial t} + (u\eta)_x - w = 0 \qquad \text{on} \qquad z = 0, \tag{5.1}$$

in which we have applied continuity to absorb a higher-order term associated with w. Collecting terms up to $O(\delta)$ for the tangential-stress condition and $O(\epsilon)$ for the normal-stress condition, we have

$$\frac{1}{\mathscr{R}_e}[u_z + \eta u_{zz} + w_x] = \frac{\sigma_x}{\mathscr{W}_e} + \frac{\mathscr{B}_o}{\mathscr{R}_e} u_{xx} \qquad \text{on} \qquad z = 0, \tag{5.2}$$

and

$$-p + \frac{\eta}{\mathscr{F}_r^2} + \frac{2}{\mathscr{R}_e} w_z = \eta_{xx}\left[\frac{\sigma}{\mathscr{W}_e} + \frac{\mathscr{B}_o}{\mathscr{R}_e} u_x\right] \qquad \text{on} \qquad z = 0. \tag{5.3}$$

From (5.3), it is clear that $\mathscr{F}_r \sim O(\epsilon^{1/2})$, and we have assumed $\mathscr{W}_e \geqslant O(1)$, $\mathscr{M}_a \leqslant O(1)$ and have relaxed the order of $\mathscr{B}_o$. These are consistent with properties of realistic bulk-phase fluids and surfactants (see for example Edwards *et al.* 1991). Note that for a clean surface, the above result to leading order reduces to $w = 0$ and $u_z = 0$ for the kinematic- and tangential-stress conditions respectively, which are equivalent to those for a free-slip surface.

From (5.1) and (5.2), the free-surface vorticity ω_s can be obtained as

$$\omega_s = u_z + \eta u_{zz} - w_x = -2\eta_{xt} - 2\eta u_{xx} - 2\eta_{xx} u - 4\eta_x u_x + \frac{\mathscr{R}_e}{\mathscr{W}_e}\sigma_x + \mathscr{B}_o u_{xx}. \tag{5.4}$$

In the right-hand side of (5.4), the first term is associated with vorticity production due to free-surface unsteadiness, the second to fourth terms correspond to free-surface advection effects resulting from the convective term in the kinematic boundary condition (5.1). In particular, the third term, $-2\eta_{xx}u$, is the well-known 'curvature effect' (Batchelor 1967; Lugt 1987) which can be derived using a stationary free surface. Such vorticity production due to surface convection was included in the computations of Dommermuth & Yue (1990) intuitively. Nevertheless, they neglected the higher-order term $w_z\eta$ in the boundary condition (5.1) ($w_z\eta = -u_x\eta$ leads to $(u\eta)_x$ in place of the linearized term $u\eta_x$). Their kinematic condition is thus inconsistent and is a cause of their difficulty in conserving the mean free surface. The last two terms in (5.4) represent respectively the Marangoni and viscous effects of the surfactant and are absent for a clean surface.

Assuming the surfactant concentration to be $O(1)$, the linearized surfactant transport equation reduces from (3.2) and (3.3) to

$$\frac{\partial \gamma}{\partial t} + (u\gamma)_x - \frac{\gamma_{xx}}{\mathscr{P}_e^s} = -\frac{1}{\mathscr{P}_e}\frac{1}{\mathscr{K}}\left[\frac{\partial c}{\partial z}\right]_{z=0}. \tag{5.5}$$

Such a linearized equation has been used in linear analyses of wave damping by surfactants (see, for example, van den Tempel 1965).

6. Numerical method and implementation

The continuity and Navier–Stokes equations ((2.1)–(2.3)) together with the surfactant-transport equations ((3.1), (5.5)), subject to the weakly nonlinear free-

surface boundary conditions on $z = 0$ ((5.1)–(5.3)) are solved numerically as an initial-boundary-value problem. The numerical scheme for the free-surface hydrodynamics problem is based on a primitive-variables formulation of the Navier–Stokes equations with spectral and finite-difference discretizations in the horizontal and vertical dimensions respectively. Continuity is enforced by solving a pressure Poisson equation in a vertically staggered grid system. Normal-stress free-surface condition (5.3) is used as Dirichlet condition for the Poisson equation. To evaluate z-derivatives of u (e.g. u_{zz}) at the free surface, the tangential-stress condition (5.2) is used. The free-surface elevation $\eta(x,t)$ is updated by integrating the kinematic free-surface condition (5.1). The computational domain is closed by imposing periodic conditions on the two vertical boundaries far away, and by a free-slip boundary on the bottom (with homogeneous Neumann condition for the pressure). A third-order Runge–Kutta method is used for time integrating the Navier–Stokes equation and the kinematic free-surface condition. The scheme is shown to conserve accurately the mean free surface, mass and energy.

For soluble surfactant transport, we adopt a numerical scheme similar to that of Pierson & Whitaker (1976). The surface-concentration transport equation (5.5) is integrated in time via a third-order Runge–Kutta scheme. The bulk-phase concentration on the free surface $c(x,0,t)$ is then obtained by combining the adsorption kinetics (3.4) (or (3.6) for nonlinear kinetics) and the diffusive flux (right-hand side of (5.5)), after expressing $\partial c/\partial z$ by finite difference. The surfactant concentration is assumed to remain constant at the truncated bottom ($c(x, z = -h, t) = 1$). With Dirichlet conditions on the free surface and bottom, the bulk-concentration transport equation (3.1) is also integrated using a Runge–Kutta scheme.

Miller (1981) solved a similar initial-boundary-value problem with diffusion-controlled adsorption isotherms. He proposed a numerical scheme wherein the substrate bulk concentration at the surface, $c(x,0,t)$, is substituted for the surface concentration γ in the surface-transport equation (5.5) using the equilibrium isotherm. The transport equation (5.5) then becomes the boundary condition for the bulk-concentration-transport equation (3.1). In contrast to Miller's scheme, the present method can be applied to any adsorption isotherm without iterations, in particular for nonlinear isotherms for which $\mathrm{d}\gamma/\mathrm{d}c$ cannot be determined explicitly. Furthermore, Miller's scheme cannot be extended to non-equilibrium kinetics. For validation, we have also implemented Miller's scheme for Henry (linear) and Langmuir (nonlinear) isotherms. The results of the concentration profiles and surfactant evolutions for these cases are graphically identical for both schemes.

7. Interaction between a free surface and a vortex pair

As a canonical problem for understanding the interaction mechanisms between a vortical flow and a free surface, we consider a vortex pair, symmetric about a vertical plane, rising vertically and impinging on the free surface. The initial vortical flow is composed of two counter-rotating vortices with a horizontal separation of $2L$. Each vortex has circulation Γ and a Gaussian distribution with standard deviation r_c (the core radius). The peak vorticity at the centre is $\omega_c = \pm\Gamma/(\pi r_c^2)$. All distances are normalized by L and velocities by $U \equiv \Gamma/(\pi L)$, which is the translation velocity of an equivalent point-vortex pair in infinite fluid. The free surface is assumed to be flat initially.

For the computations, the initial positions of the two vortex centres are located at $(x_c, z_c) = (\pm 1, -1.5)$, the peak vorticity is $\omega_c = 4$ and the core radius is $r_c = 0.5$. The

non-dimensional parameters used are $\mathscr{F}_r^2 = 0.15$, $\mathscr{R}_e = 180$ and $\mathscr{W}_e = 20$; $\mathscr{P}_e^s = 150$, $\mathscr{M}_a = 0.1$, $\mathscr{B}_o = 0.5$ for both soluble and insoluble surfactants; and $\mathscr{P}_e = 200$, $\mathscr{K} = 0.01$, $\mathscr{T} = 1$ for the soluble surfactant. For the soluble surfactant cases, the linear kinetic expression (3.4) is used and the bulk concentration is assumed to be uniformly distributed over the bulk phase initially in §7.2. Effects of nonlinear sorption kinetics and non-uniform initial bulk concentration distributions are discussed respectively in §7.3 and §7.4.

The length and depth of the computation domain is 16 and 4 with 256 and 64 grid points respectively. The time step of the Runge–Kutta integration is 0.0025. Convergence of the simulation results has been checked systematically by decreasing both the grid size and time step, as well as varying the computational domain size. In all our computations, the maximum divergence $(u_x + w_z)$ is less than 10^{-11}, the mean free surface $(\int \eta \mathrm{d}x)$ is maintained to within 10^{-12} and total energy is conserved to within 1%.

7.1. *Clean free surface–vortex interaction*

To obtain a baseline for comparison, we consider first the case of a free surface and bulk fluid free of contamination. In particular, we would like to understand the importance of free-surface convection in the production of surface vorticity. We show in figure 3 the surface vorticity ω_s, surface elevation η and horizontal velocity u at $t = 4$ (a); and 12 (b) with and without the convection term included in (5.1). The presence of the convection term in the kinematic condition causes a slightly faster propagation of free-surface disturbances although differences in the surface horizontal velocity are small in the entire interaction. The surface vorticity, however, is significantly different in the two cases especially in the vicinity of the large free-surface trough (near $x = 1.4$). At $t = 4$, the convection produces a large negative vorticity peak near this wave trough where $\eta_{xx} > 0$ and $u > 0$ and hence negative vorticity due to the curvature term $\omega_s \sim -2u\eta_{xx} < 0$. Similar features can be seen at a later time ($t = 12$) where the free surface with the convection term has a small negative curvature ripple in the trough resulting in a positive peak superimposed onto the surface vorticity distribution. The results without the convection term, on the other hand, produce very little surface vorticity at both early and later stages of the evolution.

For a clean free surface the surface tension remains constant and its effect on surface-vorticity production is not explicit in (5.4). Surface tension appears in the normal-stress surface condition which serves as the Neumann condition for the pressure field of the bulk flow. To understand the effect of constant surface tension on the production of surface vorticity, we show in figure 4 the surface vorticity ω_s, the free-surface profile η and surface horizontal velocity u for $\mathscr{W}_e = 1$, 20 and ∞ (no surface tension) (keeping $\mathscr{F}_r^2 = 0.15$ and $\mathscr{R}_e = 180$). Varying the surface tension from vanishingly small to extremely large appears to have little effect on the surface velocity. The presence of large surface tension ($\mathscr{W}_e = 1$) merely flattens the free surface and consequently reduces somewhat the surface vorticity production.

The simulations in this section for clean free surfaces have been repeated for a broad range of Froude, Weber and Reynolds numbers (maintaining laminar conditions). It is found that for the range of low to intermediate Froude numbers for which weakly nonlinear free-surface boundary conditions are valid, the effects of the free-surface boundary layer are always very weak compared to those with surface contamination (see §7.2). The vortex pair approaches the free surface and then separates, travelling effectively parallel to the free surface. The free surface thus behaves very much like a

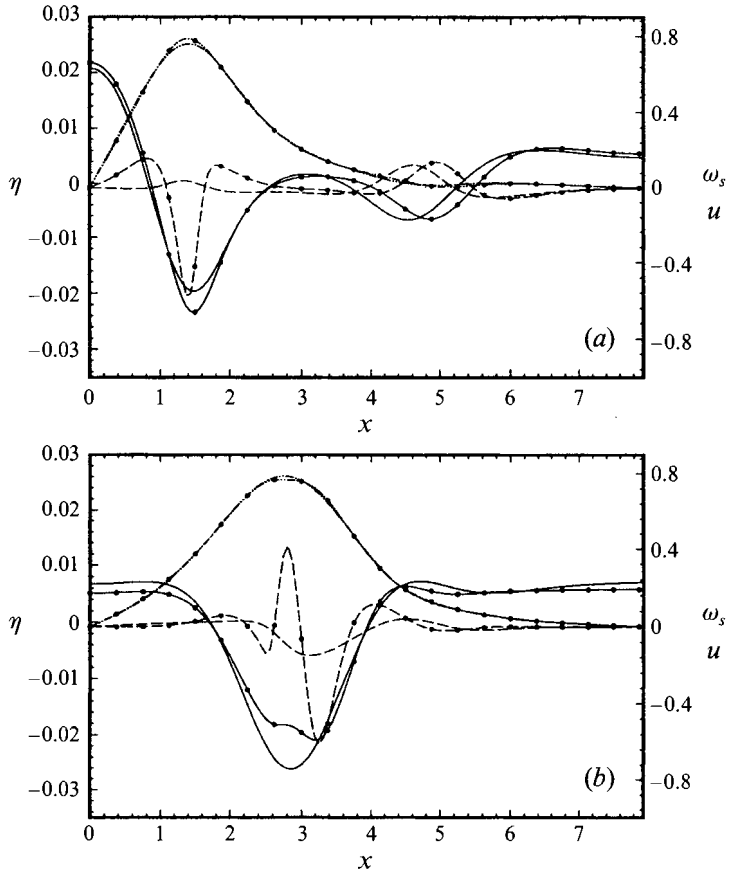

FIGURE 3. Surface vorticity ω_s (– – –), free-surface profile η (——), and surface horizontal velocity $u(x,0,t)$ (— - - — - -), with (lines with dots) and without (lines without dots) the convective term in the kinematic condition. Time $t=4$ (*a*); and 12 (*b*). ($\mathscr{F}_r^2=0.15$, $\mathscr{R}_e=180$ and $\mathscr{W}_e=20$.)

free-slip boundary — the surface shear stresses associated with a weak near-surface boundary layer being invariably small. Furthermore, *constant* surface tension has little qualitative effect on the underlying vortical flow.

7.2. *Effects of soluble and insoluble surfactants*

If the free surface is contaminated by surfactant, the Marangoni effect and viscous stresses due to the surfactant itself contribute to the production of free-surface vorticity as given by the last two terms in (5.4). Figure 5 shows the temporal evolution of the vorticity contours associated with the primary and the induced secondary vorticity for respectively the three cases of clean, insoluble-, and soluble-surfactant-contaminated free surfaces. The strong effect of surface contamination on the evolution dynamics can be seen in the magnitude of the secondary vorticity production (figure 5*b*,*c*) in contrast to the clean free-surface case (figure 5*a*). For insoluble surfactant, the secondary vorticity is strong enough to cause rebounding of the primary vortex tube. The secondary vorticity is first generated at the surface, then drawn down by the primary vortex tube, wraps around the tube and eventually forms a barrier which blocks further outward motion of the primary vortex. For the soluble surfactant case,

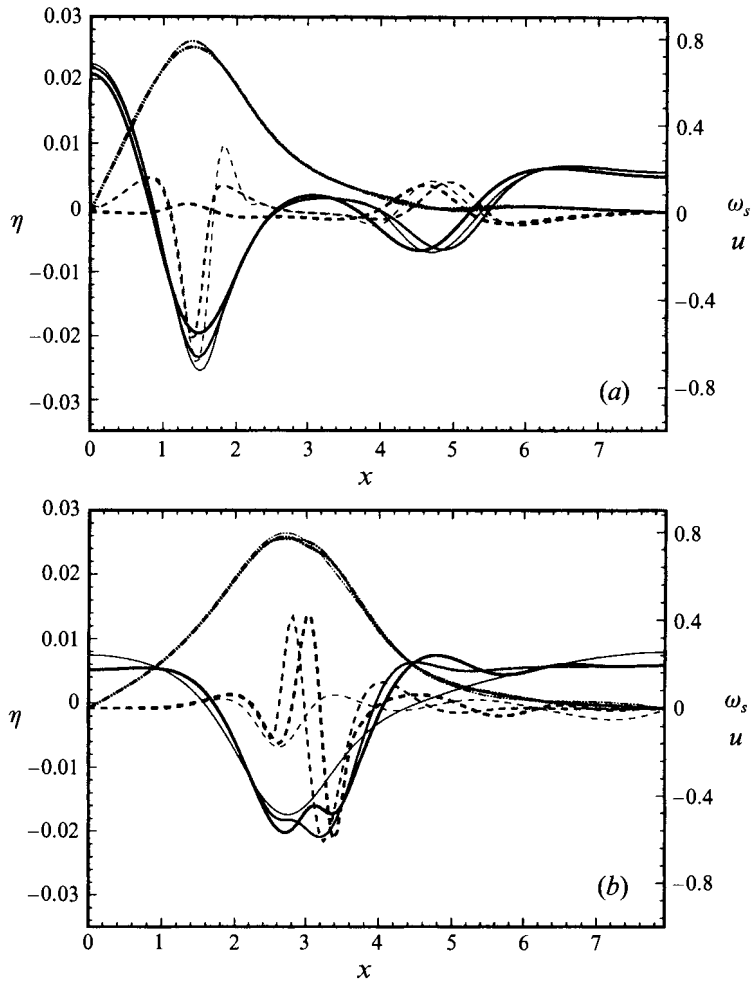

FIGURE 4. Free-surface vorticity ω_s (— — —), elevation η (———), and horizontal velocity u (—·—·—), for $We = 1$ (thin lines), 20 (medial thick lines) and ∞ (thick lines) at $t = 4$ (*a*); and 12 (*b*).

the surface vorticity generation is somewhat weakened and its effect is less dramatic than the insoluble case. As mentioned earlier, the clean free surface case resembles that of a free-slip boundary with negligible effect from the weak surface vorticity generation.

The effect of surface Marangoni and viscous stresses can also be seen in the horizontal velocities on the surface (figure 5*d–f*). For the surfactant-contaminated surfaces (figure 5*e, f*), the surface velocities are reduced compared to the clean surface flow especially in a region downstream of the moving primary vortex. This reduction is most dramatic for the insoluble-surfactant-contaminated surface (figure 5*e*) where in the region beyond the peak of the secondary vorticity the surface tangential velocity effectively vanishes.

Figure 6 shows the velocity vectors and corresponding vorticity contours at t=20 for respectively the clean, insoluble- and soluble-surfactant cases. For the insoluble surfactant, the near-surface velocities downstream of the primary vortex tube (figure

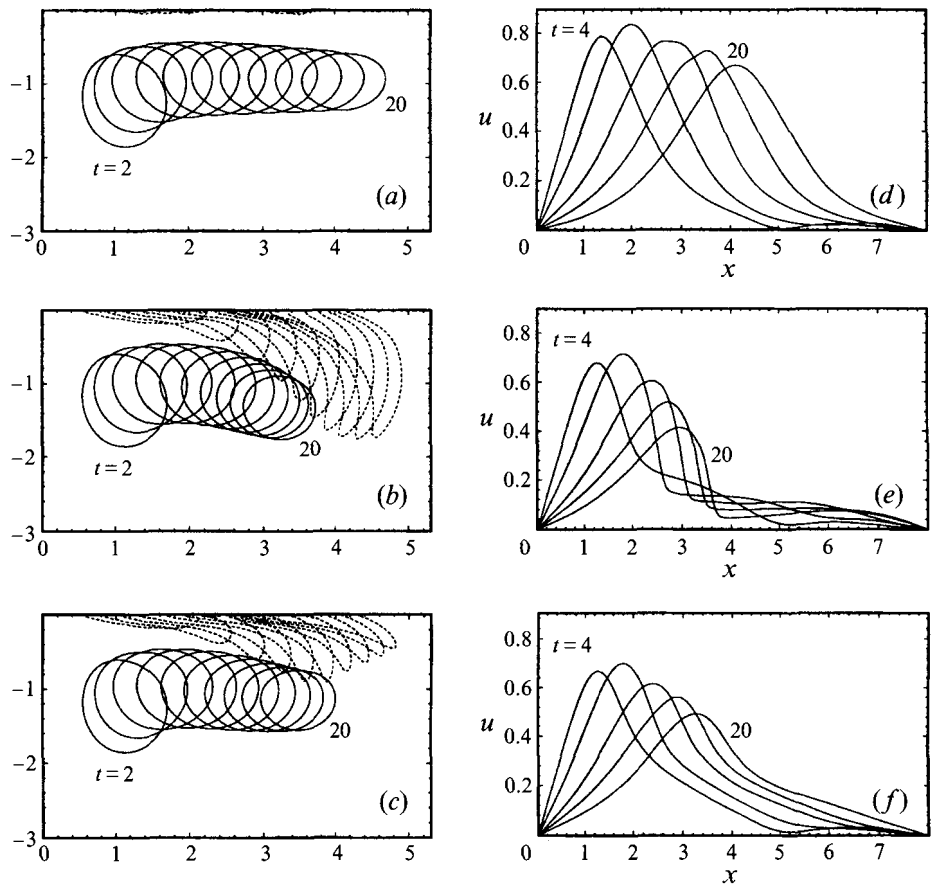

FIGURE 5. Vorticity contours of the primary ω=1 (——), and induced secondary vorticity $\omega = -0.2$ (– – –), for (*a*) clean, (*b*) insoluble-surfactant-contaminated, and (*c*) soluble-surfactant-contaminated free surfaces at $t = 2,4,\ldots,20$. The corresponding free-surface horizontal velocities $u(x,0,t)$ are shown in (*d–f*) at $t = 4, 8, 12, 16$ and 20.

6*b*) are much reduced compared to those under the clean and soluble-surfactant-contaminated surfaces (figures 6*a* and 6*c*). Such a separated boundary layer results in strong vorticity shedding (figure 6*e*) which blocks the primary vortex, causes it to rebound, and consequently reduces the induced velocities on the free surface. Such interactions are still appreciable but not as strong for the soluble-surfactant case (figures 6*c* and 6*f*) but are absent under a clean free surface (figures 6*a* and 6*d*).

The dependence of secondary vorticity production on surfactant solubility is further quantified in figure 7, which shows evolutions of the secondary vorticity circulation, Γ_s, for the clean, insoluble- and soluble-surfactant cases. The circulation Γ_s is defined in the domain $x \geqslant 0$, $\Gamma_s = \int_0^b \int_{-h}^0 \omega dz dx$ for $\omega < 0$, and b and h are half-length and depth of the computation domain respectively. For a clean surface, the induced circulation remains small throughout the interaction process. For a soluble surfactant, Γ_s decreases first and then increases. This is due to the fact that the induction of the primary vortex on the surfactant redistribution is reduced by transport between the bulk and surface surfactant. For the insoluble-surfactant case, Γ_s decreases

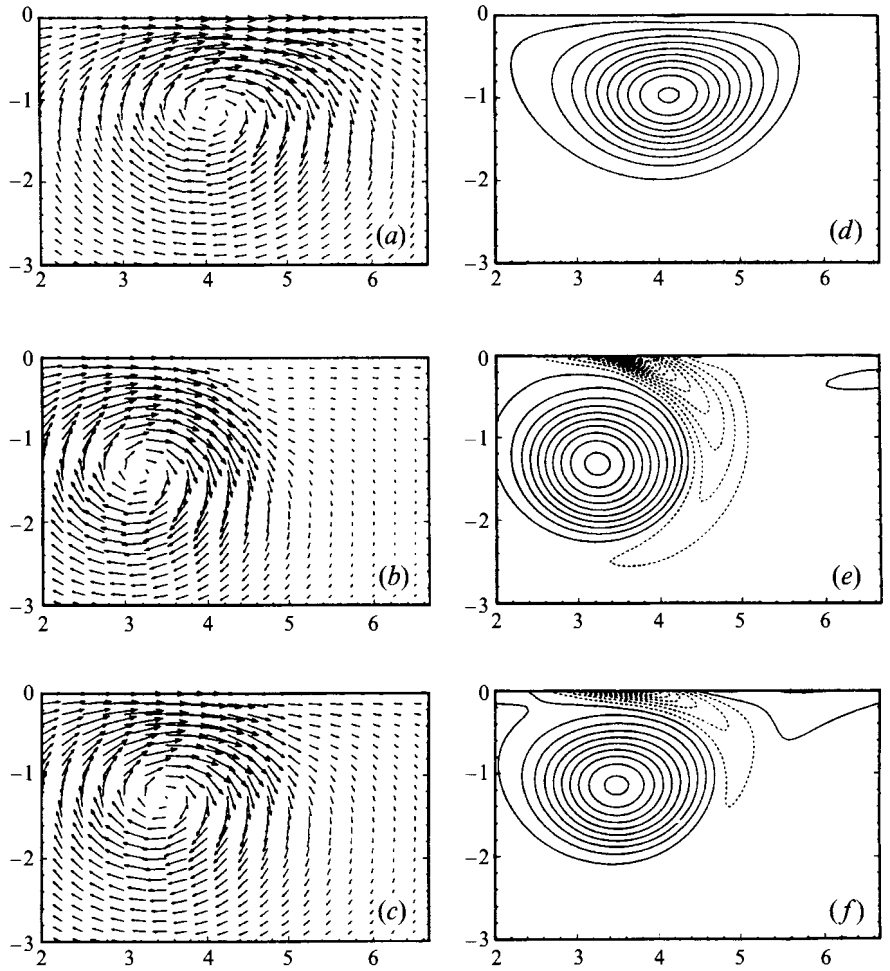

FIGURE 6. Velocity vectors and vorticity contours (dashed lines indicate negative values) at $t = 20$ for clean (a, d); insoluble-surfactant-contaminated (b, e); and soluble-surfactant-contaminated (c, f) free surfaces.

montonically even after rebounding of the primary vortex by the induced secondary vorticity.

The strong vorticity production for the contaminated surfaces and the effect of surfactant solubility are also shown in figures 8, where we plot the distributions of the surface concentration γ and the free-surface elevations η for the insoluble- and soluble-surfactant cases. For the insoluble-surfactant-contaminated surface (figure 8*a*), a surfactant 'shock' forms on the interface with a 'clean hole' near the centre and an accumulation of contamination downstream. Such a severe inhomogeneity of the surfactant distribution is caused by the large advection induced by the (primary) vortical flow. The abrupt concentration variation near the surfactant shock results in a large surface-tension gradient and consequently generates significant secondary free-surface vorticity according to (4.3) and (5.4). Near the shock front, a small free-surface hump appears (near $x \approx 3.4$ in figure 8*b*) which resembles that of a Reynolds ridge near the front of a stagnant film (see Scott 1982 — compare, for example, the

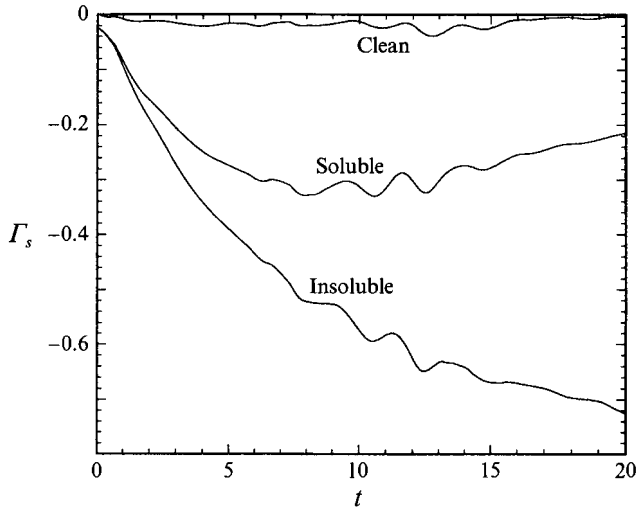

FIGURE 7. Evolutions of circulation of secondary vorticity in the domain $x \geqslant 0$, Γ_s, for clean, insoluble- and soluble-surfactant-contaminated free surfaces.

free-surface slopes near the stagnation edge of figure 8*b* to those in Scott's figure 5). Such a free-surface ridge was also noted by Hirsa & Willmarth (1994) in their experiments. This ridge-like surface deformation is, however, not present for the soluble surfactant case (figure 8*d*).

If the surfactant is soluble, the surface concentration becomes more smoothly distributed (figure 8*c*) causing a reduction of the restoring tensile stress on the surface. The milder surface surfactant gradients are a result of the vertical transport of surfactant via adsorption/desorption kinetics on the surface. Upstream of the primary vortical flow, a cleaner surface is formed as surfactant is advected out. In this region, surfactant in the bulk is adsorbed to the surface. On the downstream surface, desorption occurs which reduces the aggregation of surfactant on the surface. This vertical transport is further enhanced by the up and down swelling on respectively the upstream and downstream sides of the primary vortical flow.

The Reynolds ridge in figure 8(*a*, *b*) is an unsteady one produced over a transient vortical flow. To further elucidate the features of a Reynolds ridge, we simulate a *steady* Reynolds ridge on a contaminated free surface with a 'stagnant' surfactant distribution. We construct this steady-state flow by imposing a steady flow boundary condition on the bottom of the domain starting from an otherwise quiescent condition under an insoluble-surfactant-contaminated surface. Specifically, we choose an imposed bottom velocity which corresponds to a pair of steady Gaussian vortices *fixed* at $(x, y) = (\pm 3, -1.5)$. The peak vorticity ($\omega_c = 4$) and core radius ($r_c = 0.5$) are otherwise identical to those for the free vortices we studied above. The length and depth of the computation domain are 12 and 3 respectively and the hydrodynamic and surfactant parameters are the same as those in the transient case. Steady condition at the surface is reached after $t \approx 40$.

Figure 9(*a*) shows the surface quantities at $t = 50$. As in the transient case (figure 8*a*, *b*), a surface ridge forms near the front of the stagnant surfactant shock (at $x \approx 3.5$). The surface slope η_x changes rapidly in this region similar to that observed by Scott (1982) (a quantitative comparison can not be made since the

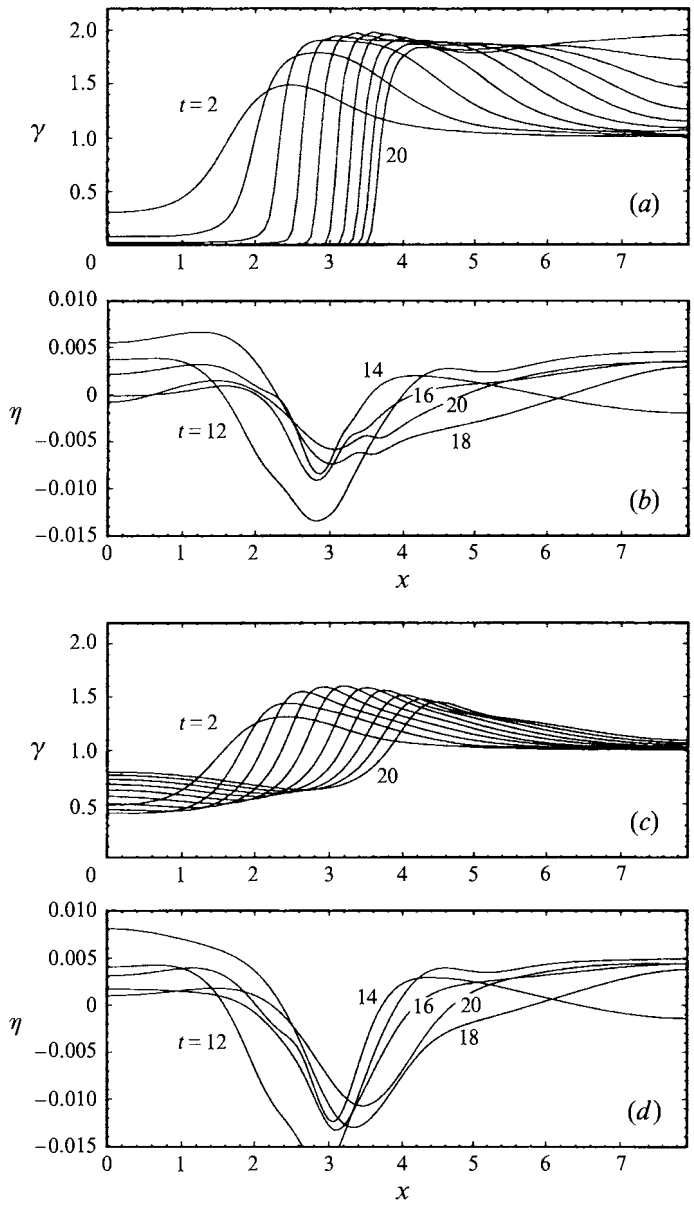

FIGURE 8. Surface concentration γ at $t = 2, 4, \ldots, 20$ and free-surface elevations η at $t = 12, 14, \ldots, 20$ for insoluble (a, b), and soluble (c, d) surfactant-contaminated free surfaces.

underlying flows in the two cases are different). Corresponding to this surface ridge and steep surfactant gradient, the free-surface vorticity exhibits a sharp (negative) peak while the surface (tangential) velocity attenuates into the region of large surface surfactant concentration. For comparison, the corresponding results for a clean free surface are shown in figure 9(*b*). The surface vorticity is very small for the clean free surface (the magnitude of maximum vorticity is only about 0.1). The most prominent differences are the attenuation of the surface elevation and velocity by the surfactant.

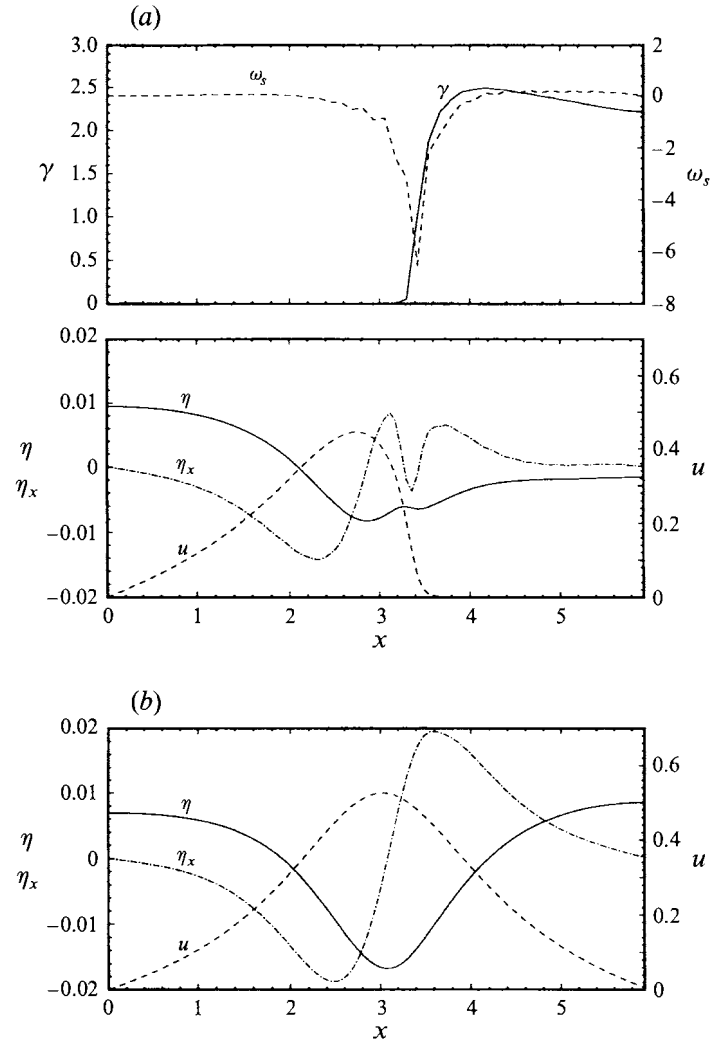

FIGURE 9. Steady-state surface concentration γ, vorticity ω_s, horizontal velocity u, elevation η and slope η_x for insoluble-surfactant-contaminated (*a*) and clean (*b*) free surfaces.

The choice of $\mathscr{W}_e = 20$ and $\mathscr{F}_r^2 = 0.15$ in our simulations in this section corresponds to a vortex pair with an initial separation of $2L \approx 6$cm with rising velocity of $U \approx 2$ m s^{-1}. These scales are representative of many of the experiments (e.g. Hirsa & Willmarth 1994). Our parameters of $\mathscr{M}_a = 0.1$ and $\mathscr{B}_o = 0.5$ for soluble and insoluble surfactants are not unrealistic for a natural film with an ideal monolayer assumption. The choice of $\mathscr{T} = 1$ with $\mathscr{K} = 0.01$ for the soluble surfactant refers to dynamic (neither diffusion nor adsorption controlled) kinetics (see §7.3) with equilibrium time (cf. figure 1*c*) $t_e \sim O(1)$, i.e. dimensional equilibrium time $T_e \sim L/U \sim O(0.01)$s. To maintain laminar conditions, our values for the bulk viscosity $\mathscr{R}_e = 180$ and surfactant diffusivities $\mathscr{P}_e = 200$ and $\mathscr{P}_e^s = 150$ are artificially low. The dependencies of the interactions on the various soluble and insoluble surfactant properties are addressed at length in §7.3.

The question remains as to whether the strong surfactant effects we show here can

be expected of flows more typical of 'prototype' scales such as may be expected in the wake of a moving body such as a ship. According to the free-surface dynamic boundary condition (2.5) and (5.2), the effect of tangential stress due to surface-tension variation is scaled by $\mathscr{W}_e^{-1}$ or $(U^2L)^{-1}$ for given surfactant/fluid properties. To check this, we repeat the simulations wherein we maintain $\mathscr{W}_e = 20$ but set $\mathscr{F}_r^2 = 0.0003$ which correspond to a problem with $2L \approx 1.4$ m and $U \approx 5$ cm s^{-1}. (In this case, $\mathscr{M}_a = 0.05$, $\mathscr{B}_o \approx 0$, and $\mathscr{R}_e = 400$, $\mathscr{P}_e^s = 200$.) Figure 10 shows the results for the clean and (insoluble) contaminated free surface cases. The effect and features due to the presence of (insoluble) surfactant are quite comparable to those observed earlier for a smaller length scale L.

7.3. *Dependence on soluble- and insoluble-surfactant properties*

The important parameters governing insoluble surfactants include surface diffusivity ($\mathscr{P}_e^s$), surface elasticity ($\mathscr{M}_a$) and surface viscosity ($\mathscr{B}_o$). Surface diffusivity serves as transport dissipation which also smooths the surfactant gradient and reduces the production of free-surface vorticity. Surface elasticity determines the magnitude of the restoring tensile stress in the tangential-stress condition (5.2) and surface-vorticity generation indicated by (5.4). The effect due to the presence of surface viscosity is less clear since $\mathscr{B}_o$ appears in both the tangential- and normal-stress conditions, (5.2) and (5.3).

Figure 11 shows the free-surface vorticity ω_s and its two main contributions due to surfactant, $\mathscr{R}_e\sigma_x/\mathscr{W}_e$ and $\mathscr{B}_o u_{xx}$, for varying $\mathscr{B}_o = 0.005$, 0.5 and 2, at $t = 4$. The underlying flow is still that induced by a rising vortex pair as in previous sections. Increasing surfactant viscosity $\mathscr{B}_o$ increases the contribution of the $\mathscr{B}_o u_{xx}$ term to ω_s production, while that associated with the Marangoni effect $\mathscr{R}_e\sigma_x/\mathscr{W}_e$ decreases. Thus there are two opposing effects of surface viscosity on free-surface vorticity production: viscous surfactant stress contributes to the shear stress at the surface and increases the vorticity production; on the other hand, surface viscosity obstructs surfactant transport, reduces the concentration gradient and consequently the vorticity generation.

For soluble surfactant, additional properties of importance are the bulk diffusivity ($\mathscr{P}_e$), equilibrium ratio between surface and bulk concentration ($\mathscr{K}$), ratio between diffusion and adsorption rates ($\mathscr{T}$), and saturation surfactant concentration (β) for nonlinear kinetics. As we saw in §7.2, for initially uniformly distributed surfactant, solubility generally diminishes the surfactant shock and weakens the free-surface boundary layer. Surfactant rupture, such as that shown in figure 8(*a*), generally does not occur if there is an adequate rate of adsorption/desorption from/to the bulk phase. The distribution of surface-adsorbed surfactant is determined by the competition among the effects of surface convection and diffusion, and surface/bulk diffusion-sorption kinetics. The transport is also influenced strongly by the up/down swellings associated with the vortical flow.

As we show in figure 1, the diffusion-adsorption ratio $\mathscr{T}$ is the most crucial among the transport properties in determining the kinetic resistance against adsorption to the surface. For low $\mathscr{T}$, the kinetics is diffusion controlled and the kinetic resistance remains constant. For high $\mathscr{T}$, the resistance against adsorption increases linearly with $\mathscr{T}$ and the kinetics are adsorption controlled. Figure 12 shows the evolutions of surface concentration for $\mathscr{T} = 0.001, 1$, and 100 which correspond respectively to diffusion-controlled, dynamic and adsorption-controlled kinetics. For low kinetic resistance ($\mathscr{T} = 0.001$), the bulk surfactant quickly diffuses to the surface where it is adsorbed. The same happens in the opposite direction, in which the surface surfactant

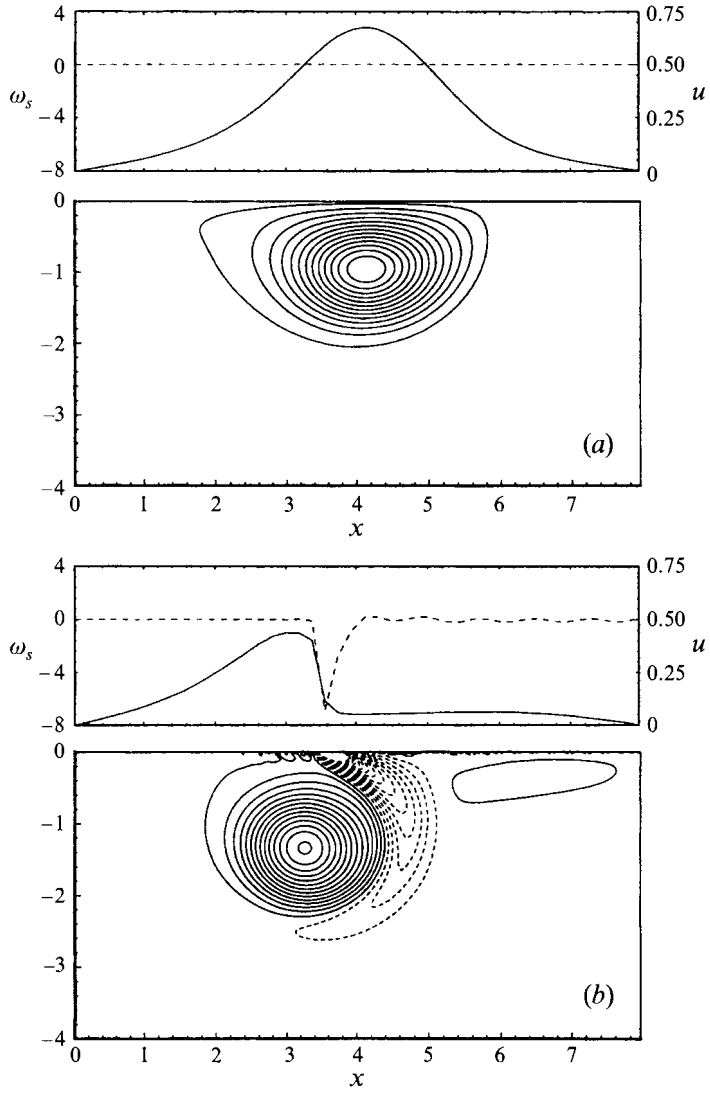

FIGURE 10. Free-surface vorticities ω_s (——), horizontal velocities u (– – –) and vorticity contours (dash lines indicate negative values) for (*a*) clean; and (*b*) insoluble-surfactant-contaminated surfaces at $t = 20$. Parameters used correspond to a physical problem with separation distance $2L \sim 1.4\,\mathrm{m}$ and rising velocity $U \sim 0.05\,\mathrm{m\,s^{-1}}$.

is desorbed and diffuses to the bulk phase. Such transport to/from the bulk phase compensates for and reduces the surface transport due to convection and diffusion. As $\mathscr{T}$ increases, the resistance against the sorption process increases. For $\mathscr{T} = 100$ (figure 12*c*), the resistance is large enough so that the surface transport is nearly independent of the bulk transport. Consequently, a sharp surfactant front forms as in the case of an insoluble surfactant. For $\mathscr{T} = 1$ (figure 12*b*), the competing sorption and diffusion rates are comparable, and the effect of solubility is between the previous two extreme kinetics.

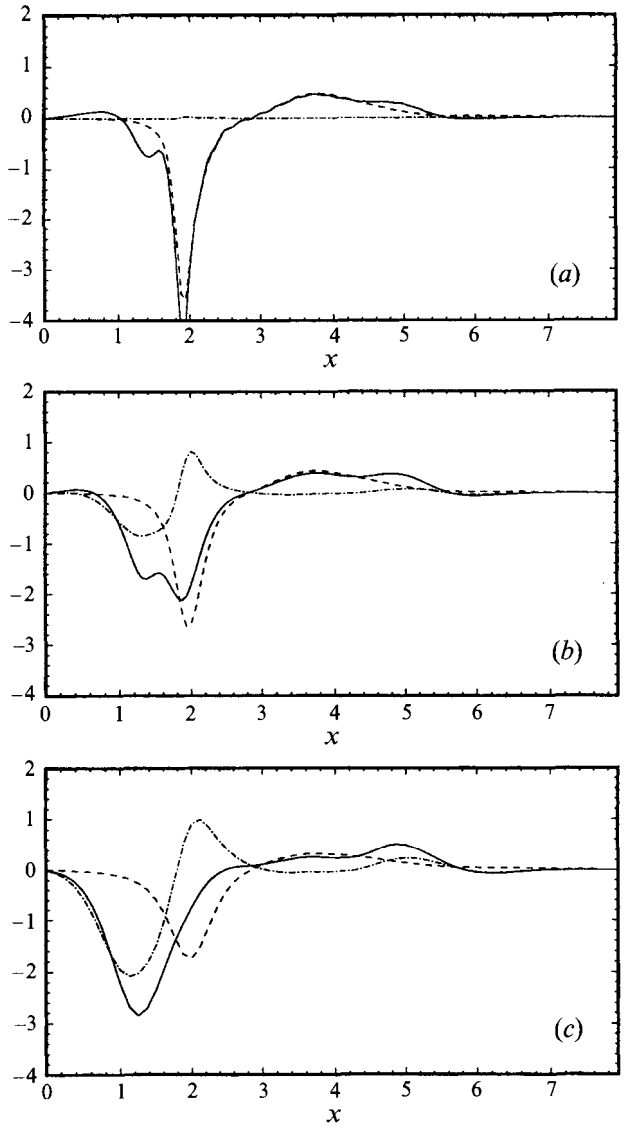

FIGURE 11. Free-surface vorticity ω_s (——), and its two main contributions due to surfactant, $\mathscr{R}_e\sigma_x/\mathscr{W}_e$ (– · – · –), and $\mathscr{B}_o u_{xx}$ (– – –), at $t = 4$ for $\mathscr{B}_o = 0.005$ (*a*); 0.5 (*b*); and 2 (*c*).

In figure 13, we show the dependence on $\mathscr{T}$ of the surface concentration dose

$$d(t) \equiv 1 - b^{-1} \int_0^b \gamma(x,t)\mathrm{d}x\,,$$

where b is the length of the (periodic) domain. Physically, $d(t)$ represents the amount of surfactant desorbed from the surface to the bulk phase. For $\mathscr{T} = 0.001$, $d(t)$ oscillates but increases continuously with time, indicating a steady desorption of the surface concentration to the bulk phase in the presence of high solubility. For $\mathscr{T} = 100$, the kinetics resist the sorption process and the total amount of surface surfactant remains almost unchanged. Between the two extremes, $\mathscr{T} = 1$, the amount

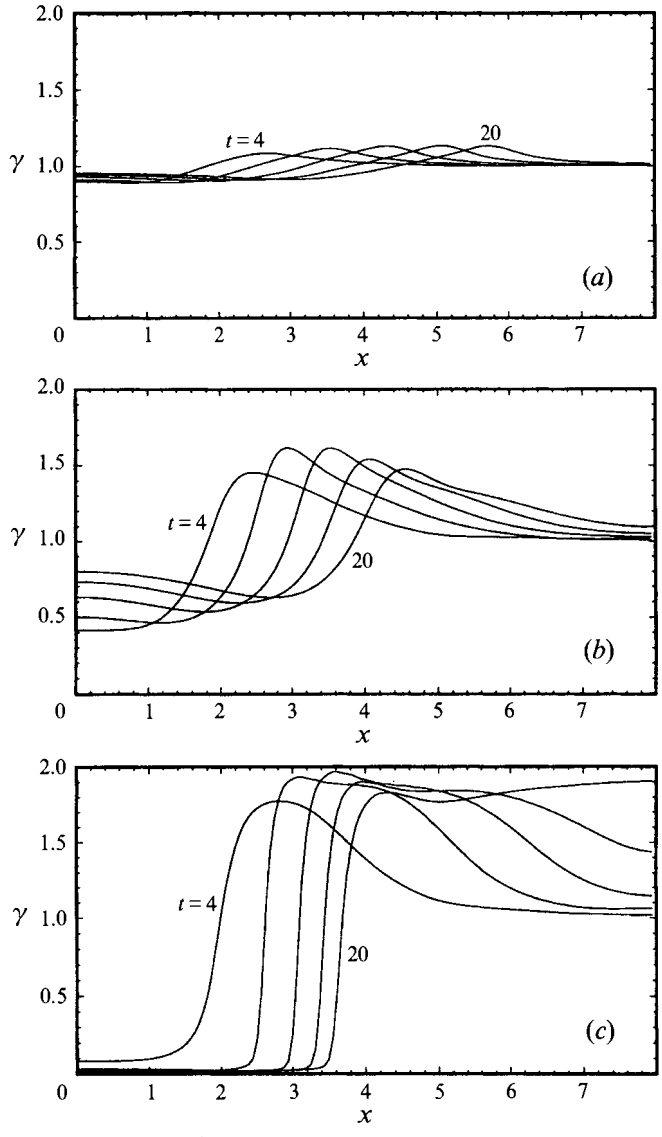

FIGURE 12. Surface surfactant concentration γ at $t = 4, 8, \ldots, 20$ for $\mathscr{T} = 0.001$ (*a*); 1 (*b*); and 100 (*c*).

of surface concentration depends on the competition among the transport processes. All our results so far for soluble surfactants are based on linear sorption kinetics ($\beta = \infty$) and the linear equation of state. Nonlinearity of the kinetic isotherm increases the sorption rate as shown in figure 1(*a*). This effect is shown in figure 13 for $\mathscr{T} = 1$ for the nonlinear kinetics. Consistent with figure 1(*a*), the concentration dose in this case increases with time in contrast to the linear kinetics.

The dependence of surface tension on surfactant composition also becomes nonlinear for nonlinear sorption kinetics according to Gibbs' equation (4.2). For the nonlinear equation of state (4.4), surface tension decreases exponentially with increasing surface concentration as the kinetics become nonlinear (see figure 2). This

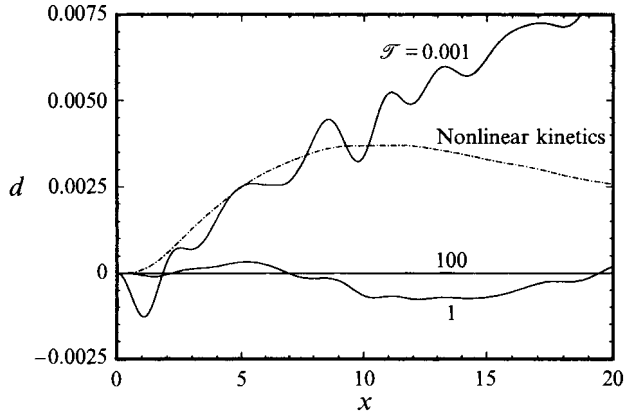

FIGURE 13. Surface concentration dose $d(t)$ for linear sorption kinetics with $\mathscr{T} = 0.001$, 1 and 100; and for nonlinear sorption kinetics (– · – · –) with $\mathscr{T} = 1$.

means that for nonlinear kinetics the restoring surface tension due to variation of the surfactant distribution increases as the concentration increases. In contrast, for linear kinetics, the resorting tension remains constant for the same concentration gradient. The effects of nonlinear sorption kinetics and the equation of state on the evolutions of the surface concentration and surface tangential velocity are shown in figure 14. For comparison, the corresponding evolutions for linear kinetics are also plotted. The most prominent difference is the much slower propagation of the nonlinear kinetics surfactant front and consequently the surfactant does not pile up. Such a difference in surface transport between linear and nonlinear kinetics is primarily a result of increasing restoring tensile stress with concentration for the nonlinear kinetics which causes the surface to become stiffer as soon as the surfactant gradient forms. Such stiffness slows down the hydrodynamic convection on the free surface (see figure 14*b*) and reduces the transport of surfactant.

7.4. *Effect of initial stratification of the bulk (soluble) surfactant*

Our results so far for soluble surfactant assume an initially uniform bulk concentration, i.e. $c(x, z, t = 0) = 1$. In such cases, the bulk phase serves as a surfactant reservoir which smooths out the variations in the surface concentration and generally diminishes surfactant effects as compared to the insoluble case. This situation is not necessarily true if the (initial) bulk surfactant concentration is not uniform. To understand this, we consider the same problem of the rising vortex pair in a fluid with an initial vertically stratified bulk concentration. Specifically, we consider two types of vertical stratification: a contaminated bulk layer next to the free surface with clean water below, and a layer of clean water next to the surface with surfactant concentration below. For the purpose of numerical simulations, the initial concentrations are assumed to have the form

$$c(x, z, t = 0) = \frac{1}{2}\left[1 \pm \tanh\left(\frac{z + H}{0.1}\right)\right],$$

where the positive/negative sign corresponds to a contaminated/clean bulk fluid layer next to the free surface, and H measures the thickness of the top-contaminated/clean layer. The initial surface concentration remains the same ($\gamma(x, t = 0) = 1$) in all cases.

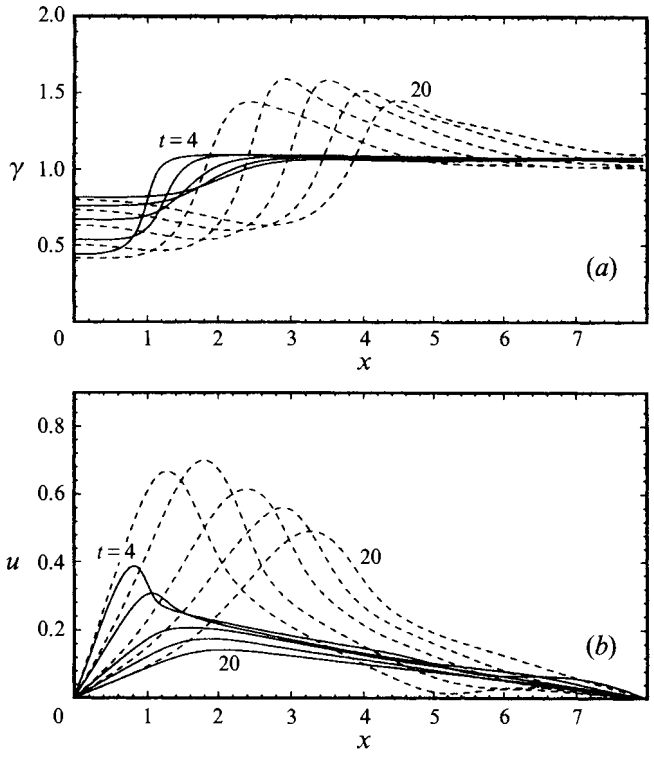

FIGURE 14. Surface surfactant concentration γ (a); and horizontal velocity $u(x,0,t)$ (b) at $t = 4, 8, \ldots, 20$ for nonlinear (——) and linear (– – –) sorption kinetics. ($\beta = 0.1$ and $\mathscr{T} = 1$).

Figure 15 shows the evolution of the surface horizontal velocities $u(x,0,t)$ and the vorticity contours at $t = 20$ for initially top-contaminated stratification with respectively $H = 2$ ('thick') and $H = 0.5$ ('thin') surfactant layers. For comparison, the uniform bulk concentration case considered earlier is also plotted. The Marangoni effect is clearly enhanced for this type of stratification. As expected, the effect is more pronounced for the thinner initially contaminated bulk layer. In this latter case, the reduction of the free-surface horizontal velocity and production of surface vorticity are in fact more similar to those for the insoluble surfactant case (cf. figures 5 and 6). The corresponding surface concentration $\gamma(x,t)$ and substrate surface concentration $c(x,0,t)$ evolutions are shown in figure 16. For the thin stratified layer case, a portion of the free surface is swept clean as the underlying bulk surfactant is exhausted. The surface concentration features are not unlike those in figure 8(a) for insoluble surfactant. The thick surfactant layer evolutions are generally in between the uniform and thin stratification results. These features can be explained from contour (grey-scale) plots of the bulk concentration, shown in figure 17. The amplification of (surface) surfactant effect as the bulk contamination thickness is decreased is clearly seen. The primary vortical flow produces an upwelling of (eventually) clean water near the centre which enhances the creation there of a low surface concentration region.

The stratification effects are quite different when the initial bulk distribution is reversed, i.e. when the surface surfactant and (uniform) bulk surfactant are separated by a layer of clean water. Figure 18 shows this case for H=0.5 and 2. In contrast

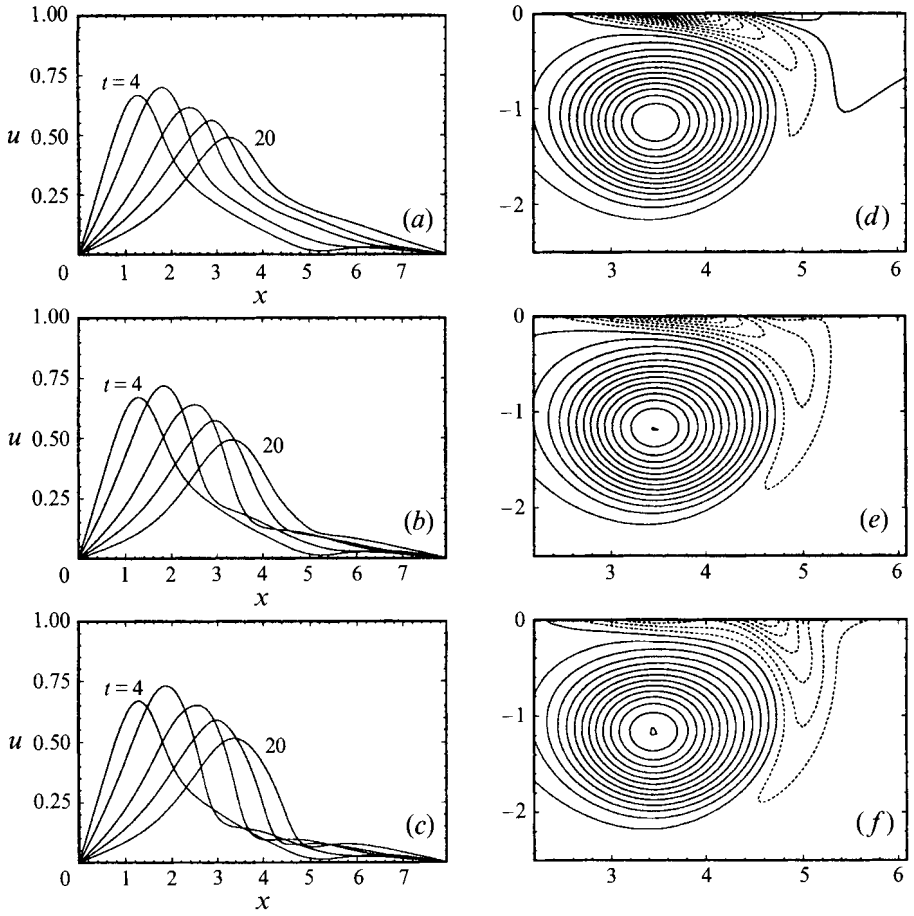

FIGURE 15. Surface horizontal velocities $u(x, 0, t)$ at $t = 4, 8, \ldots, 20$ and vorticity contours (dash lines indicate negative values) at $t = 20$ for initially uniform (a, d), and stratified bulk contamination near the free surface with H=2 (b, e) and 0.5 (c, f).

to the previous case, the horizontal velocities downstream of the primary vortex are now increased and are in fact greater than those on a clean surface (cf. figure 5*d*). Looking at the vorticity contours, we see that in addition to the secondary vorticity, tertiary vorticity with the same rotational sign as the primary vortex is produced further downstream on the free surface. The surfactant distributions on the surface evolve very differently from what we have seen so far. The downstream surface remains clean while the surfactant is accumulated by advection (figure 19). Two steep surfactant fronts form on both sides of the region where the surfactant is aggregated. The generation of tertiary vorticity observed in figure 18 is due to the presence of the surfactant slope facing downstream. Contours of the bulk concentration (figure 20) reveal its role in the overall evolution. The primary vortical flow causes an upwelling of bulk contamination into the initially clean bulk region, eventually reaching the free surface to create a distinct front which then generates the tertiary vorticity. It is also clear that a deeper initially clean layer between the free surface and uniform bulk concentration below intensify such reversed surfactant effects.

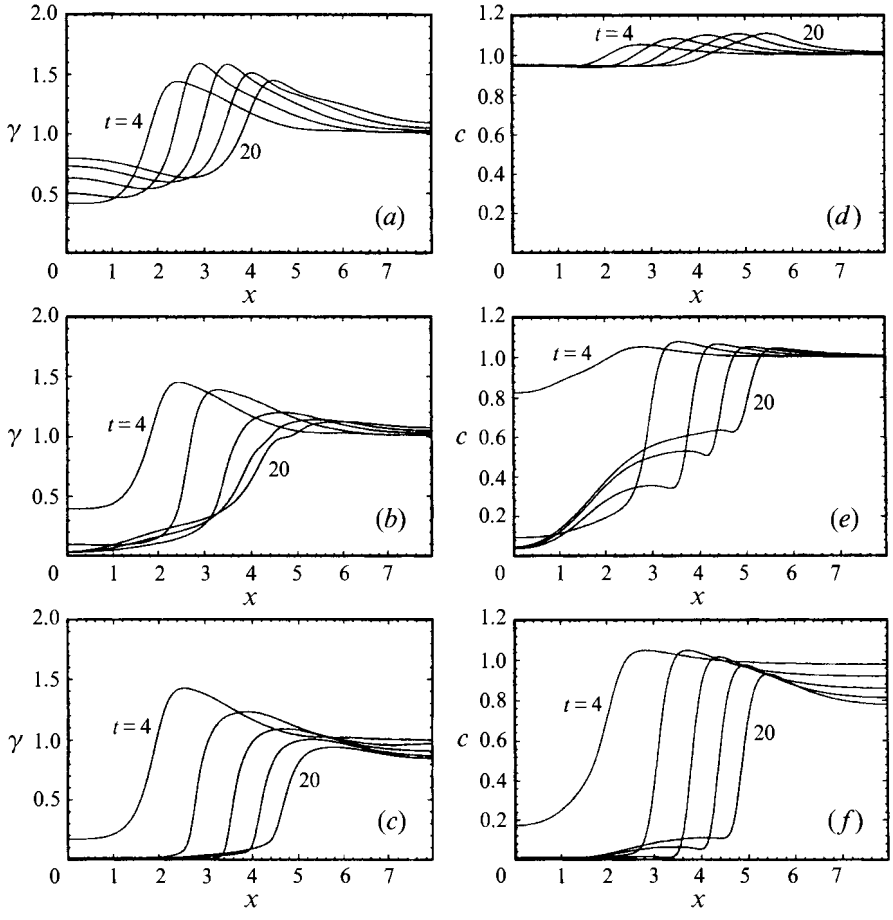

FIGURE 16. Surface concentration $\gamma(x,t)$ and bulk concentration on the surface $c(x,0,t)$ at $t = 4,8,\ldots,20$ for initially uniform (a,d), and stratified bulk contamination near the free surface with $H=2$ (b,e) and 0.5 (c,f).

One way to further quantify the effect of surfactant stratification is to consider the evolution of the total secondary vorticity generation, measured, say, by its circulation, Γ_s (in the domain $x \geqslant 0$). Figure 21 shows such evolutions for different initial surfactant stratifications. For comparison, the result for a uniform bulk concentration case is also plotted. It is clear that, measured from the production of secondary vorticity, top contamination develops a stronger surfactant effect with the negative circulation $-\Gamma_s$ increasing with decreasing surfactant depth H. The opposite is true for bottom contamination which produces less (negative) secondary vorticity as H increases. The result for uniform initial concentration is between the two stratified cases. These trends are consistent with expectation once the physics associated with figures 17 and 20, for example, are understood.

8. Interaction between a free surface and a shear flow

An important area of interest is the effect of surfactants on the near-surface wake behind a moving body. To study this, we consider as a canonical problem surfactant

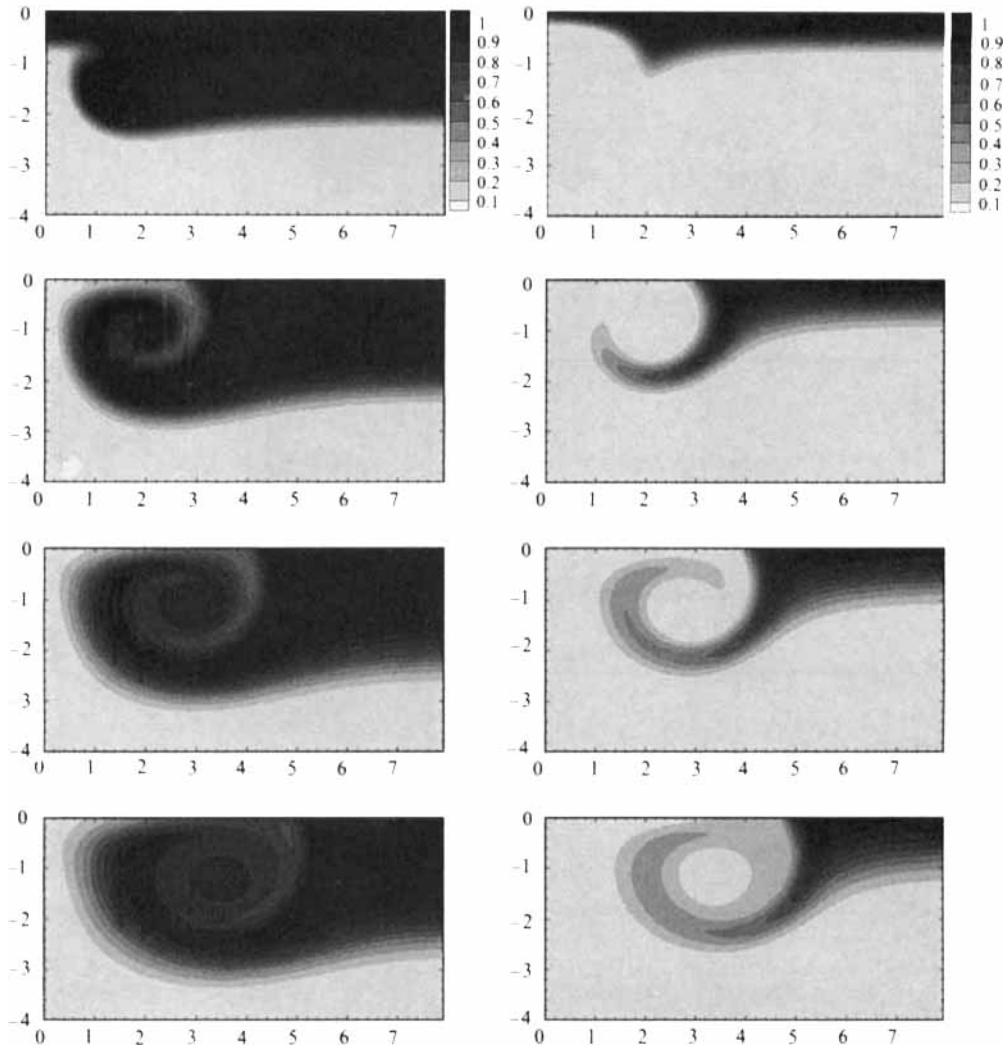

FIGURE 17. Bulk concentration $c(x, z, t)$ for initially stratified bulk contamination near the free surface for $H = 2$ (left column) and 0.5 (right column) at $t = 2, 8, 14$ and 20.

effects on the evolution of a free-surface shear flow. Following Triantafyllou & Dimas (1989), we start with a two-dimensional shear flow corresponding to that immediately behind a NACA 0003 hydrofoil (Mattingly & Criminale 1972):

$$u(z, t) = 1 + (u_c - 1)\mathrm{sech}^2(k_0 z),$$

where we have normalized lengths by the characteristic depth of the shear layer and velocities by the free-stream velocity of the parallel flow. The values of the profile parameters used are $u_c = 0.0012$ and $k_0 = 0.88137$ so that $(1 - u)/(1 - u_c) = 0.5$ at $z = -1$. To trigger the unstable evolution, we perturb the flow by superimposing an unstable mode obtained from linear stability analysis (Triantafyllou & Dimas 1989). According to this analysis, there are two different classes of unstable modes corresponding respectively to low (mode I) and high (mode II) wavenumbers for the present low Froude number simulations.

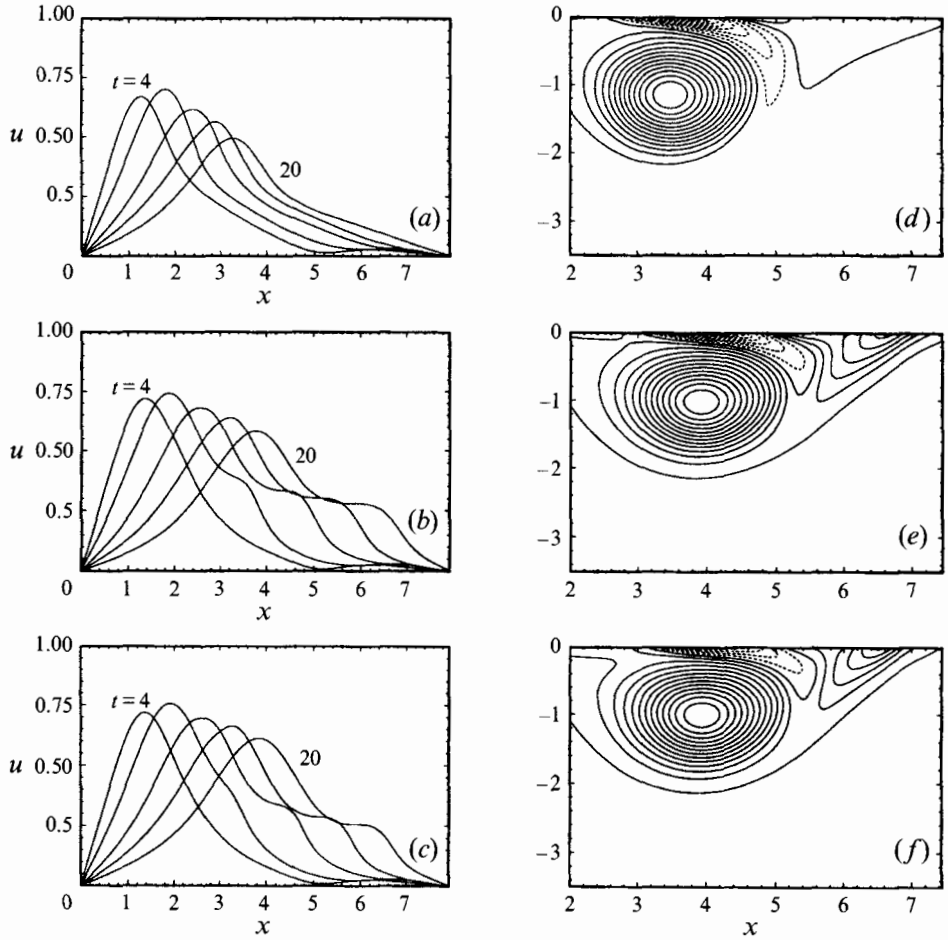

FIGURE 18. Free-surface horizontal velocities $u(x,0,t)$ at t=4,8,...,20 and vorticity contours (dash lines indicate negative values) at $t = 20$ for initially uniform (a,d), and stratified bulk contamination away from the free surface with H=0.5 (b,e) and 2 (c,f).

Figure 22 shows the evolutions of the vorticity field for a mode I instability case (wavenumber $k = 0.4$) for respectively clean, insoluble and soluble surfactant. The parameters of the problem are $\mathscr{F}_r = 0.5$, $\mathscr{R}_e = 300$, $\mathscr{P}_e^s = 300$, $\mathscr{B}_o = 0.5$ and $\mathscr{M}_a = 0.2$. For soluble surfactant, $\mathscr{P}_e = 300$ and linear adsorption kinetics are used with $\mathscr{K} = 0.01$, $\mathscr{T} = 1.0$, and the initial bulk concentration is uniform. The computation domain is $2\pi/k$ by 8 deep with 128 grid points in each direction. In the early stage of the evolution ($t = 40$), the unstable perturbation grows in a similar manner for all three cases with the exception of somewhat stronger secondary vorticity production for the contaminated flows. As time increases, however, variations of the surface surfactant concentration resulting from the velocity fluctuations lead to significant generation of free-surface secondary vorticity. This vorticity eventually interacts/interferes with the growing mode in the primary shear flow leading to qualitatively distinct features for all three cases. At a late time ($t = 400$) for the clean free surface, the shear flow instability has ceased to grow owing to viscous dissipation. For the insoluble surfactant flow, the secondary vorticity wraps around

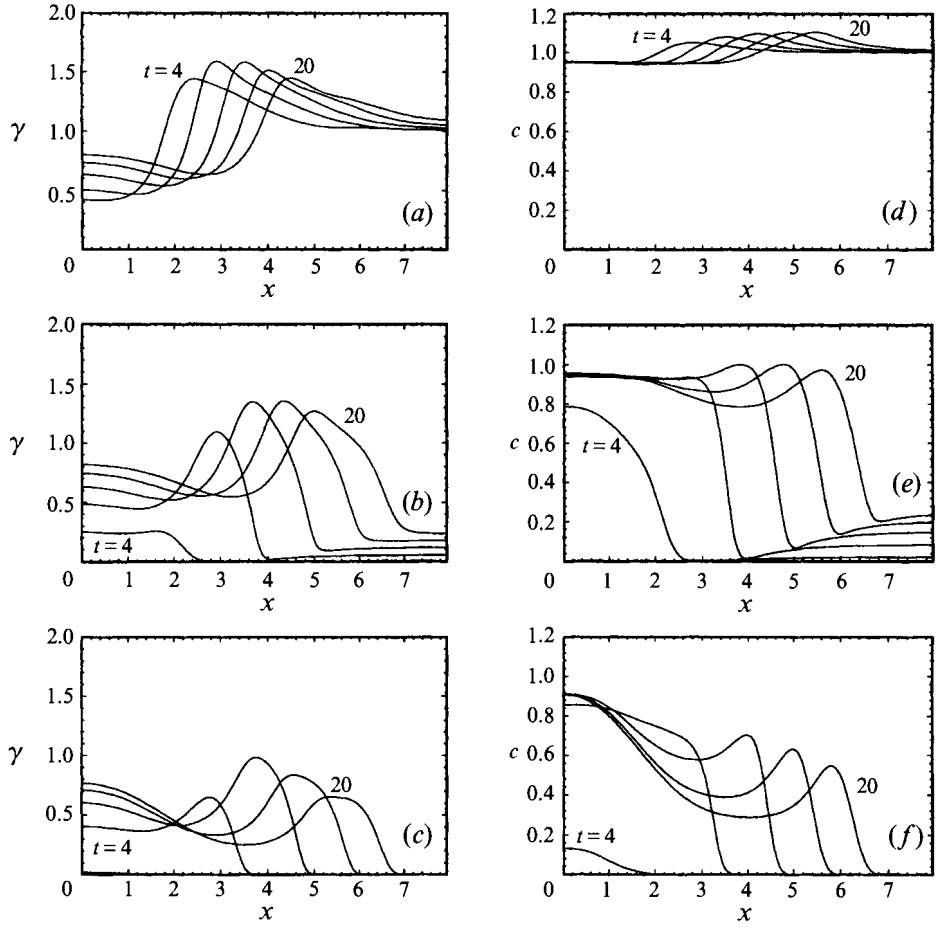

FIGURE 19. Surface concentration $\gamma(x,t)$ and bulk concentration on the surface $c(x,0,t)$ at $t = 4,8,\ldots,20$ for initially uniform (a,d), and stratified bulk contamination away from the free surface with H=0.5 (b,e) and 2 (c,f).

and pushes down on the primary perturbed flow vortex. Above the secondary vortex, a strong tertiary vortex with the same sign as the primary vortex forms beneath the free surface. For the soluble case, the effect is diminished by surfactant absorption/desorption, and the vortical structure of the (clean) primary flow is still somewhat preserved.

We show in figure 23 the free-surface elevation η, vertical velocity w and surfactant concentration γ (for the contaminated surfaces) at an intermediate time $t = 280$. For the clean free surface, a non-sinusoidal elevation with a pronounced trough is observed and is in fairly good agreement with the inviscid simulation results of Dimas & Triantafyllou (1994) (see also Dimas 1991). For the insoluble surfactant case, a small hump in the surface elevation corresponding to a Reynolds ridge can be observed near the surfactant front at $x \approx 1$ and is clearly revealed in the surface vertical velocity. The soluble surfactant results are qualitatively more similar to the clean flow with a slight shift in the phase of the main features. The overall understanding and conclusions about the effects of insoluble and soluble surfactants are thus consistent with what has been obtained for the vortex pair interaction problem (§7).

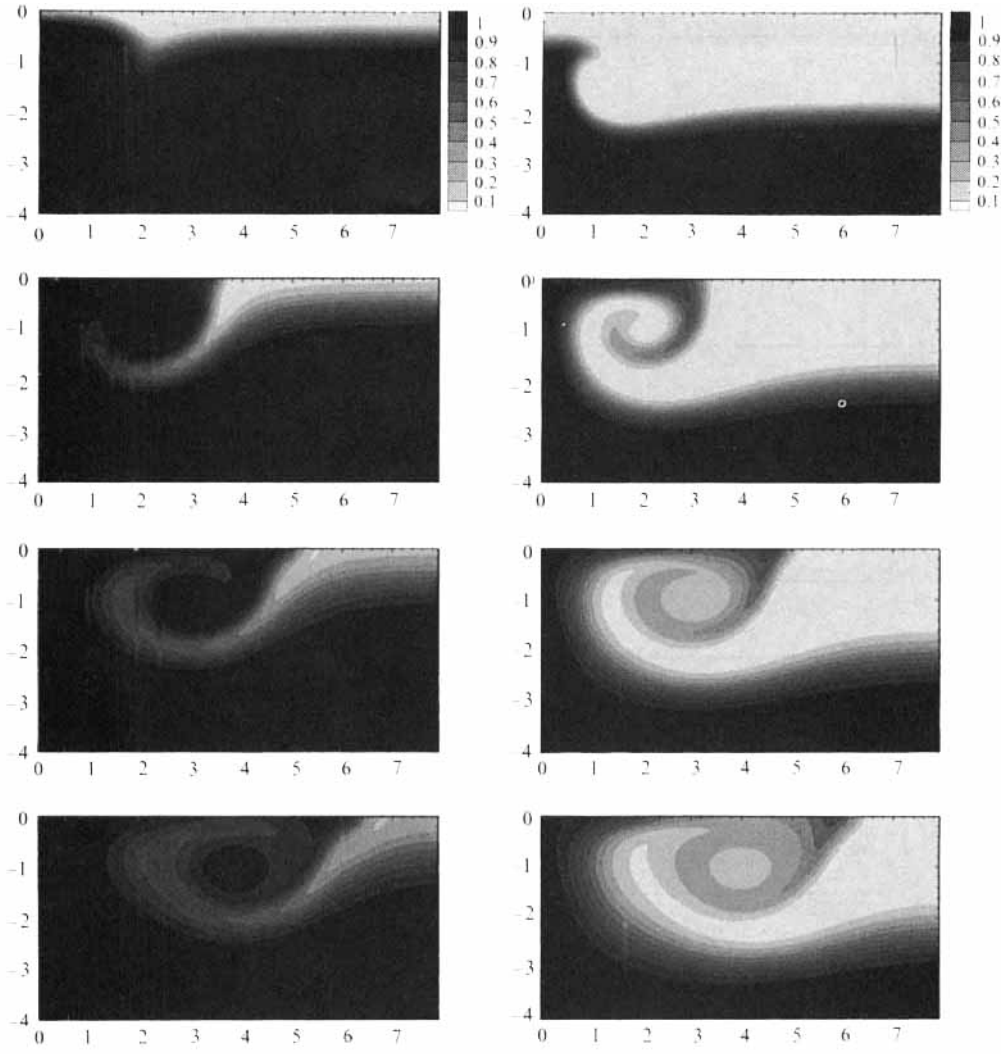

FIGURE 20. Bulk concentration $c(x, z, t)$ for initially stratified bulk contamination away from the free surface for $H = 0.5$ (left column) and 2 (right column) at $t = 2, 8, 14$ and 20.

Finally, we show the results for a mode II unstable ($k = 2$) flow in figure 24. The parameters are $\mathscr{F}_r = 1.5$, $\mathscr{R}_e = 400$, $\mathscr{P}_e = 400$, $\mathscr{P}_e^s = 400$, $\mathscr{B}_o = 0.1$, $\mathscr{M}_a = 2.0$, $\mathscr{K} = 0.005$ and $\mathscr{T} = 0.01$. According to the inviscid simulation (for clean water) (Dimas & Triantafyllou 1994), such a mode II perturbation grows slowly and eventually reaches saturation leading to a quasi-steady flow. These evolution characteristics are also seen in the present simulation results for viscous flows. The vortical structures under clean, insoluble- and soluble-surfactant-contaminated surfaces all reach saturated states after $t = 30$ as figure 24 shows. The surfactant effects for such a mode II unstable shear flow are substantially different from those of mode I instability or the vortex pair in §7. In this case the submergence of the unstable shear flow is of the same order as the wavelength of the instability and the vortical flow associated with the instability is relatively weak. As the flow approaches an equilibrium state, the surfactant distributions for the insoluble and soluble cases likewise approach steady

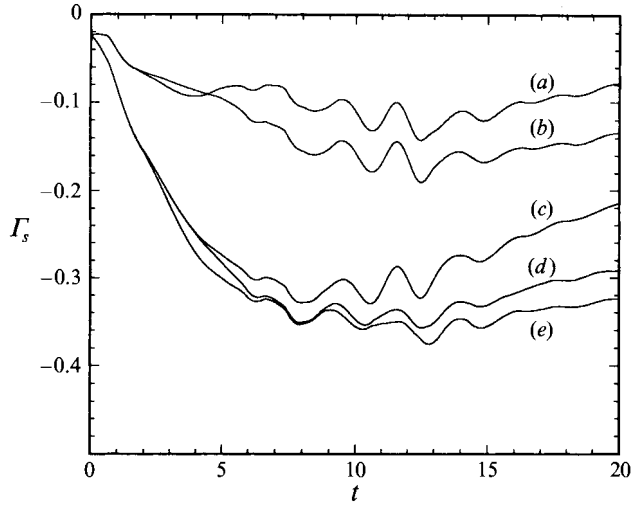

FIGURE 21. Evolutions of circulation of secondary vorticity Γ_s for bottom contamination with $H = 2$ (*a*), 0.5 (*b*), initially uniform distribution (*c*), and top contamination with $H = 2$ (*d*), 0.5 (*e*).

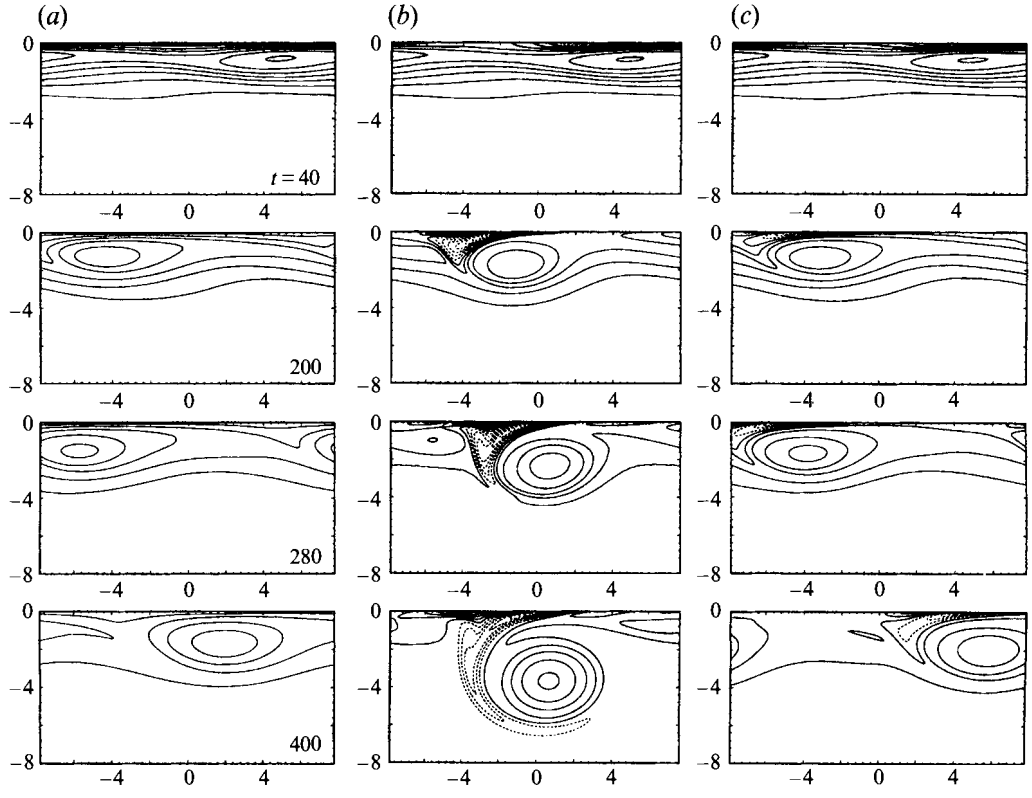

FIGURE 22. Vorticity contours (dash lines indicate negative values) for a mode I unstable shear flow at $t = 40, 200, 280$ and 400 for (*a*) clean; (*b*) insoluble-surfactant-contaminated; and (*c*) soluble-surfactant-contaminated free surfaces.

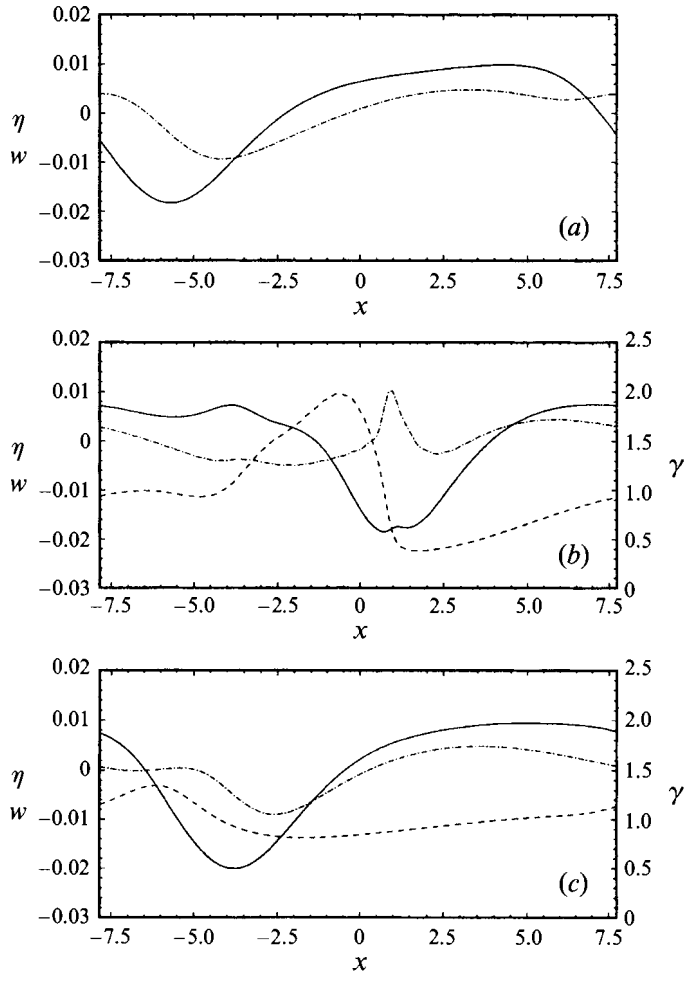

FIGURE 23. Free-surface elevation η (——), vertical velocity w on the free surface (– · – · –), and surface surfactant concentration γ (– – –) at $t = 280$ for (*a*) clean; (*b*) insoluble-surfactant-contaminated; and (*c*) soluble-surfactant-contaminated free surfaces.

states and cease to generate free-surface vorticities. In contrast to the cases studied earlier, there are no strong interactions between the near-surface and submerged vortical flows.

The findings in this section further elucidate the closed-loop interaction of the Marangoni effect. For mode I instability, the unstable waves develop strong oval-shaped vortices below the free surface (see figure 22*a*, also Dimas & Triantafyllou 1994). These vortices cause redistribution of surfactant on the free surface which in turn produces strong secondary vorticity and changes the structure of the primary vortical flow. On the other hand, mode II instability develops into much weaker vorticity compared to mode I. The induced surfactant variation is milder and the associated surface vorticity generation is weak. Consequently, the primary unstable mode eventually reaches a quasi-steady state.

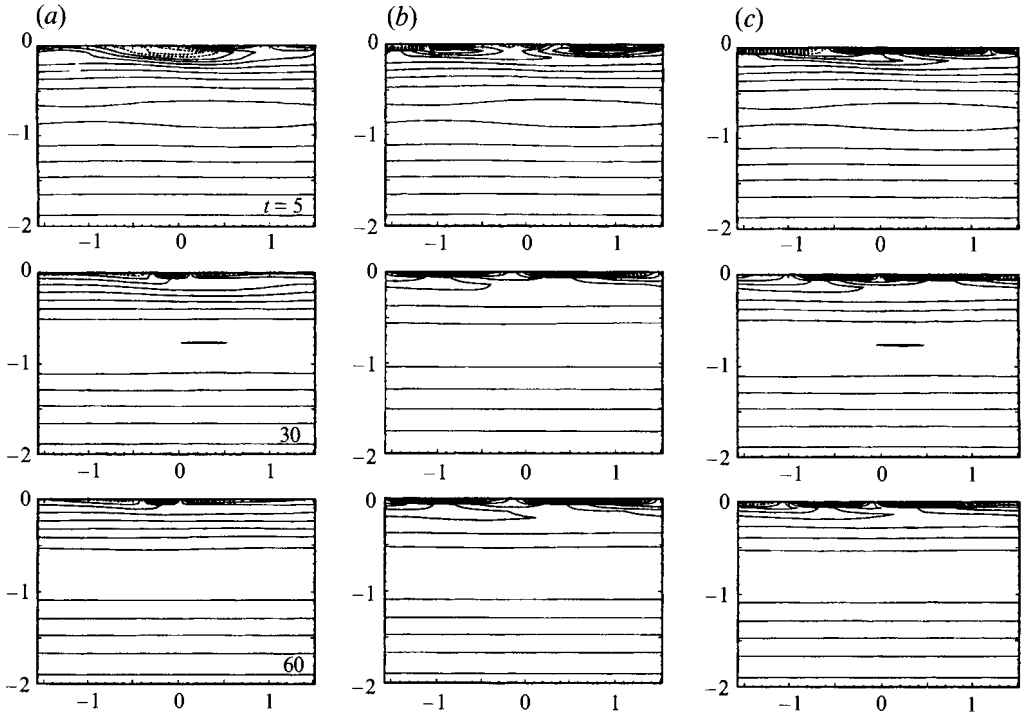

FIGURE 24. Vorticity contours (dash lines indicate negative values) for a mode II unstable shear flow at $t = 5, 30$ and 60 for (*a*) clean; (*b*) insoluble-surfactant-contaminated; and (*c*) soluble-surfactant-contaminated free surfaces.

9. Conclusion

We consider the effects of soluble and insoluble surfactants on laminar free-surface vortical flows. A quantitative description is presented and a numerical model developed which include the convection-diffusion-sorption processes governing the evolutions of bulk and surface surfactant concentrations and their coupling to the free-surface vortical flow dynamics through the stress boundary conditions. Two canonical vortical flows are considered: a pair of vortex tubes impinging the free surface and an evolving unstable shear flow beneath the free surface.

Our numerical results display and quantify the closed-loop interactions between the surfactant and the underlying vortical flows. For small to moderate Froude number motions under a clean free surface, surface vorticity production (due to curvature and unsteadiness) is small and the effect of the free surface is generally insignificant, somewhat similar to a free-slip surface. In the presence of even a small amount of surfactant, the Marangoni effect associated with variations in the surfactant concentration dominates the surface vorticity generation. Significant surface vorticity can be produced leading to strong interactions with the underlying flow. Since the surfactant transport is itself a result of the flow, the coupled interaction dynamics can be quite varied. The effects are generally in between, but qualitatively distinct from, either a no-slip or free-slip boundary. If the surfactant is soluble (and the kinetics is not absorption controlled), surfactant effects are generally diminished for (initially) uniform bulk concentrations. When stratification of the bulk concentration is considered, however, the evolution dynamics becomes even more complicated and

surfactant effects may be completely changed and even amplified relative to the insoluble case.

A main objective of this study is to investigate the implications of the presence of contamination on free-surface vortical and turbulent flows in the laboratory and in the ocean. The present results show that depending on the local variation in surfactant concentration, the nature of stress boundary conditions on the free surface can vary from that of effectively free-shear to almost no-slip. This has a direct effect on the nature of near-surface turbulent fluctuations on a microscopic scale. Since variations in the surfactant concentration have in general temporal and spatial scales of the order of the flow itself, the macroscopic flow-scale structures near the free surface must necessarily also be modified. Such effects should play an important role in observable small- to medium-scale coherent flow structures near the surface.

This research was sponsored by the Office of Naval Research under the Fluids Mechanics Program (contract N00014-94-1-0075), and under a University Research Initiative on Free-Surface Vortical Flow (contract N00014-92-J-1610). WTT was also supported by a grant (NSC 84-2611-M-019-012) from the National Science Council of the Republic of China. Most of the computations were performed on Cray Y-MP computers at the Naval Oceanographic and Atmospheric Research Laboratory, at Cray Research, Inc., and at the Taiwan Ocean University.

REFERENCES

ALPERS, W. & HÜHNERFUSS, H. 1989 The damping of ocean waves by surface films: a new look at an old problem. *J. Geophy. Res.* **94**, 6251–6265.

BARGER, W. R. 1991 A review of experimental observations and remaining questions concerning formation, persistence, and disappearance of sea slicks. *Naval Research Laboratory NRL Rep.* 9313.

BARKER, S. J. & CROW, S. C. 1977 The motions of two-dimensional vortex pairs in a ground effect. *J. Fluid Mech.* **82**, 659–671.

BATCHELOR, G. K. 1967 *An Introduction to Fluid Dynamics.* Cambridge University Press.

BERNAL, L. P., HIRSA, A., KWON, J. T. & WILLMARTH, W. W. 1989 On the interaction of vortex rings and pairs with a free surface for various amounts of surface active agent. *Phys. Fluids* A**1**, 2001–2004.

BORWANKAR, R. P. & WASAN, D. T. 1983 The kinetics of adsorption of surface active agents at gas-liquid surfaces. *Chem. Engng Sci.* **38**, 1637–1649.

DIMAS, A. A. 1991 Nonlinear interaction of shear flows with a free surface. PhD thesis, MIT, Department of Ocean Engineering.

DIMAS, A. A. & TRIANTAFYLLOU, G. S. 1994 Nonlinear interaction of shear flow with a free surface. *J. Fluid Mech.* **260**, 211–246.

DOMMERMUTH, D. G. & YUE, D. K. P. 1990 A numerical study of three-dimensional viscous interactions of vortices with a free surface. In *Proc. 18th Symp. Naval Hydro., Ann Arbor, MI*, pp. 727–788.

EDWARDS, D. A., BRENNER, H., & WASAN, D. T. 1991 *Interfacial Transport Processes and Rheology.* Butterworth-Heinemann.

GAINES, G. L. 1966 *Insoluble Monolayers at Liquid-Gas Interface.* Interscience.

HARPER, J. F. 1974 The motion of bubbles and drops in liquids. In *Proc. Intl. Colloqu. on Drops and Bubbles., Pasadena, CA*, pp. 300–303.

HIRSA, A., TRYGGVASON, G., ABDOLLAHI-ALIBEIK, J. & WILLMARTH, W. W. 1990 Measurement and computations of vortex pair interaction with a clean or contaminated free surface. In *Proc. 18th Symp. Naval Hydro., Ann Arbor, MI*, pp. 521–531.

HIRSA, A. & WILLMARTH, W. W. 1994 Measurement of vortex pair interaction with a clean or contaminated free surface. *J. Fluid Mech.*, **259**, 25–45.

LUCASSEN, J. 1982 Effect of surface-active material on the damping of gravity waves: a reappraisal. *J. Colloid Interface Sci.* **85**, 52–58.

LUCASSEN-REYNDERS, E. H. 1981 Adsorption at fluid interfaces. In *Anionic Surfactants* (ed. E.H. Lucassen-Reynders), pp. 1–54. Marcel Dekker.

LUGT, H. J. 1987 Local flow properties at a viscous free surface. *Phys. Fluids* **30**, 3647–3652.

MATTINGLY, G. E. & CRIMINALE, W. O. 1972 The stability of an incompressible two-dimensional wake. *J. Fluid Mech.* **51**, 233–272.

MILLER, R. 1981 On the solution of diffusion controlled adsorption kinetics for any adsorption isotherms. *Colloid & Polymer Sci.* **259**, 375–381.

PIERSON, F. W. & WHITAKER, S. 1976 Studies of the drop-weight method for surfactant solutions I. mathematical analysis of the adsorption of surfactants at the surface of a growing drop. *J. Colloid Interface Sci.* **54**, 203–218.

SCOTT, J. C. 1982 Flow beneath a stagnant film on water: the Reynolds ridge. *J. Fluid Mech.* **116**, 283–296.

SCRIVEN, L. E. 1960 Dynamics of a fluid interface. *Chem. Engng. Sci.* **12**, 98–108.

TEMPEL, M. VAN DEN 1965 Damping of waves by surface-active materials. *J. Chem. Phys.* **42**, 2769–2777.

TRIANTAFYLLOU, G. S. & DIMAS A. A. 1989 Interaction of a two-dimensional separated flow with a free surface at low Froude numbers. *Phys. Fluids* A**1**, 1813–1821.

TRYGGVASON, G., ABDOLLAHI-ALIBEIK, J., WILLMARTH, W. W. & HIRSA, A. 1992 Collision of a vortex pair with a contaminated free surface. *Phys. Fluids* A**4**, 1215–1229.

WANG, H. T. & LEIGHTON, R. I. 1990 Direct calculation of the interaction between subsurface vortices and surface contaminants. In *Proc. 19th Intl. Conf. Offshore Mechanics and Arctic Engineering, Houston, TX*, pp. 271–277.

YEUNG, R. & ANANTHAKRISHNAN, P. 1992 Vortical flows with and without a surface-piercing body. In *Proc. 19th Symp. Naval Hydro., Seoul, Korea.*